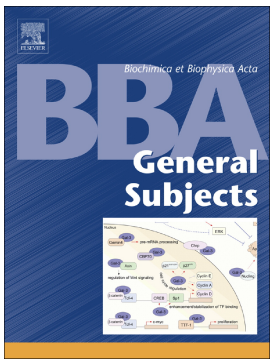

Biological activity of quinazoline analogues and molecular modeling of their interactions with G-quadruplexes

Jose Kaneti, Milena Georgieva, Miroslav Rangelov, Irena Philipova, Bela Vasileva, Ivan Angelov, Dessislava Staneva, George Miloshev, Snezhana Bakalova

PII: S0304-4165(20)30284-1

DOI: https://doi.org/10.1016/j.bbagen.2020.129773

Reference: BBAGEN 129773

To appear in: *BBA - General Subjects*

Received date: 30 June 2020

Revised date: 17 September 2020

Accepted date: 20 October 2020

Please cite this article as: J. Kaneti, M. Georgieva, M. Rangelov, et al., Biological activity of quinazoline analogues and molecular modeling of their interactions with G-quadruplexes, *BBA - General Subjects* (2020), https://doi.org/10.1016/j.bbagen.2020.129773

Biological Activity of Quinazoline Analogues and Molecular Modeling of their Interactions with G-quadruplexes

Jose Kaneti,[I] Milena Georgieva,[II] Miroslav Rangelov,[I] Irena Philipova,[I] Bela Vasileva,[II] Ivan Angelov,[I] Dessislava Staneva,[II] George Miloshev,[II] Snezhana Bakalova[I]*

[I] *Institute of Organic Chemistry with Centre of Phytochemistry, Bulgarian Academy of Sciences, 1113 Sofia, Bulgaria*

[II] *Laboratory of Yeast Molecular Genetics, Institute of Molecular Biology "Roumen Tsanev", Bulgarian Academy of Sciences, 1113 Sofia, Bulgaria*

** Corresponding author*

ORCID: 0000-0001-9142-2281, Jose Kaneti

ORCID: 0000-0002-2371-7544, Milena Georgieva

ABSTRACT

- *Background:*

Quinazolines **1** to **6**, with an aromatic or aryl-vinyl substituent in position 2 are selected with the aim to compare their structures and biological activity. T*h*e selection includes a natural alkaloid, schizocommunin, and the synthetic 2-(2'-quinolyl)-3H-quinazolin-4-one, known to interact with guanine-quadruplex dependent enzymes, respectively telomerase and topoisomerase.

- *Methods:*

Breast cancer cells of the MDA cell line have been used to study the bioactivity of the tested compounds by the method of Comet Assay and FACS analyses. We model observed effects assuming stacking interactions of studied heterocycles with a naked skeleton of G-quadruplex, consisting of guanine quartet layers and potassium ions. Interaction energies are computed using a dispersion corrected density functional theory method, and an electron-correlated molecular orbital theory method.

- *Results:*

Selected compounds do not remarkably delay nor change the dynamics of cellular progression through the cell cycle phases, while changing significantly cell morphology. Our computational models quantify structural effects on heterocyclic G4-complex stabilization energies, which directly correlate with observed biological activity.

- *Conclusion*

Our computational model of G-quadruplexes is an acceptable tool for the study of interaction energies of G-quadruplexes and heterocyclic ligands, predicting, and allowing design of novel structures.

- *General significance:*

Genotoxicity of quinazolin-4-one analogues on human breast cancer cells is not related to molecular metabolism but rather to their interference with G-quadruplex regulatory mechanisms. Computed stabilization energies of heterocyclic ligand complexes of G-quadruplexes might be useful in the prediction of novel telomerase / helicase, topoisomerase and NA polymerase dependent drugs.

KEYWORDS: Quinazoline analogues; genotoxicity; breast cancer cells; G-quadruplex molecular modeling; DFT, MP2, and RIMP2 calculations; G-quadruplex ligand stabilization energies

1. *Introduction*

Numerous plant and marine medicines with quinazoline components have been known to Asian folk practitioners for time immemorial. Presently, more than 220 natural alkaloids possess a quinazoline or quinazolinone fragment, and the interest in this class of compounds is steadily growing due to their broad and diverse biological activity and medicinal applicability.[1-3] Quinazoline heterocycles are structurally closely similar to a number of biologically active compounds, extending to the basic carriers of biological hereditary information, namely purines and pyrimidines as nucleic acid (NA) bases.[1, 2] Quinazolin-4-ones are among the conveniently accessible heterocycles, frequently using the long known Niementowski synthesis.[1-4] The latter heterocyclic molecules provide sufficient variability in the search for biologically potent compounds of prospective medicinal interest.[1-5] We have used aldol type conversions of 2-alkylsubstituted quinazolin-4-ones[6] looking for structural and topological similarities with nucleic acid base pairs,[5-9] so that enhanced activity of potential novel derivatives might be expected beforehand.

There are a couple of important details of structural requirements to potentially biologically active molecules related to NA base pairs. First, it is the capability to form intra- and inter- molecular hydrogen bonds like the in-plane interactions of NA base pairs. The second requirement is the capability to participate in dispersion interactions of the type of stacking interactions between NA base pairs within the NA helix. With heterocyclic 2-substituted quinazolin-4-one analogues, both requirements are easy to satisfy, as is obvious with planar heterocyclic compounds **1 – 6** shown in the Scheme 1 below, possessing at least one proton donor – acceptor pair of atoms including nitrogen.

The naturally occurring schizocommunin **3** has been extensively studied aiming first at the clarification of its structure as a quinazoline derivative.[7] More recently, **3** and its derivatives have been found to react specifically with DNA in telomeres and thus to affect a deepest mechanism of cell proliferation and apoptosis by stabilization of guanine quadruplexes, G4, and thus inhibiting telomerase.[8] Pyridine and quinoline substituted quinazolin-4-ones **5** and **6** are known,[5] and have also been reported as physiologically active, interacting with another guanine-quadruplex related enzyme, topoisomerase.[9-11] In this study, we design and synthesize the novel molecules **1** and **2**, as well as **4**, which is an aza-derivative of **3**. Then we use the opportunity to investigate the biological activities of these four as well as of the two relatively well-known compounds, **5**, and **6**, in relation to

their primary structural characteristics. Our results indicate that all listed compounds induce DNA damage of different extent depending on their structure on human breast cancer cells. In addition, the studied quinazoline analogues bring changes in the overall cellular morphology of the tested cells. We further use computational modeling of shown quinazolin-4-one derivatives **1 – 6**, and attempt to find connections of theoretical quantities to the biological activity of the compounds. As far as mechanisms of the observed biological effects of **3**, **5**, and **6** have already been discussed, [7-12] this might open possibilities to develop potential drugs based on heterocyclic compounds designed preliminarily. On the other hand, correspondence of model expectations for chosen heterocycles and experimentally registered effects may in turn contribute to understanding of biochemical mechanisms, and possibly direct further design of promising heterocyclic structures.

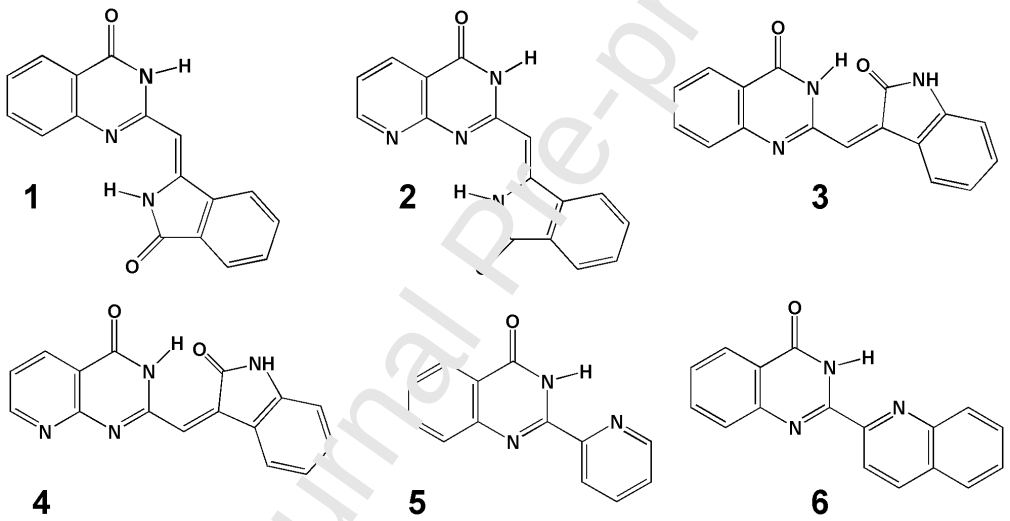

Scheme 1: Selected aromatic quinazoline analogues with potential for NH--N and NH--O intra- and inter- molecular hydrogen bonding, as well as for stacking interactions of planar heterocycles with nucleic acid bases.

Our chosen selection logic for molecules, capable of hydrogen bonding and NA stacking, limits the range of eligible structures to aromatic or quasi-aromatic heterocycles while evidently including the growing set of natural aromatic alkaloids, known for many useful biological effects. [12]

2. *Biological activity*

2.1. *2-Substituted analogues of quinazolin-4-one induce genotoxic stress on MDA cells*

Human breast cancer cells of the MDA cell line have been used as a model to study the bioactivity of the tested compounds. The cells have been treated with compounds **1** to **6**, Scheme 1, for 4 hours at 37°C. To test the genotoxic potential of the six tested substances we have performed the method of Comet assay, also called single-cell gel electrophoresis (SCGE). SCGE sensitively and precisely detects all kinds of damages in DNA including single-strand DNA breaks, double-strand DNA breaks and alkaline labile sites.[13-15] The method is renowned with its sensitivity as it allows measurement of DNA damage at the level of single cells.[16, 17] We have performed the neutral variant of the method.[18, 19] It is recognised for its high sensitivity allowing detection of DNA breaks at much lower concentrations than its alkaline variant.[19] MDA cells were treated with compounds **1** to **6** in concentrations of 30, 75 and 150 μg/ml for 4 hours at optimal conditions and after that were subjected to SCGE. Representative images of nuclei (cells without DNA damage) and comets (i.e. cells with damaged DNA) are shown on Figure 1.

As a control for DNA damage we have used 5mM hydrogen peroxide (H_2O_2) for 30 min at 37°C. We have detected extensive DNA damage in 100% of the observed objects under the fluorescent microscope, and therefore have assumed it as a positive control for genotoxicity. The six tested compounds showed dose-dependent genotoxicity resulting in appearance of long comets with high intensity of DNA in the tail (Fig. 1). Comet Assay data are quantified by the CometScore software. The parameter "Olive Tail Moment" (OTM) is one of the most reliable parameters in SCGE data analysis that gives representative and precise estimation of the level of genotoxicity of the tested substances. OTM is generally calculated as a product of two factors: the percentage of DNA in the tail and the distance between the mass intensity center of the comet head and the tail along the x-axis of the comet.[20] MDA cells treated with the studied substances and with H_2O_2 show extensive DNA damage at all tested concentrations. We have prepared two controls: negative control, cells without treatment with genotoxins and positive – H_2O_2-treated cells. This allows setting the thresholds for lack and presence of DNA damage, respectively green and red dotted lines on Figure 2. Following the red dotted threshold one can easily see that at concentrations of 75 and 150 μg/ml all compounds induced comet tails in the cells with compounds **2**, **3** and **4**

demonstrating the highest genotoxic activity. The two 2-aza-aromatic substituted quinazoline derivatives **5** and **6** exhibited moderate genotoxicity at the lowest tested concentration which is easily seen from the morphology of the detected comet images. The same has been observed for compound **1**. The genotoxicity effect for the latter three compounds, as shown on Fig. 1, was not as robust as observed for **2**, **3** and **4**.

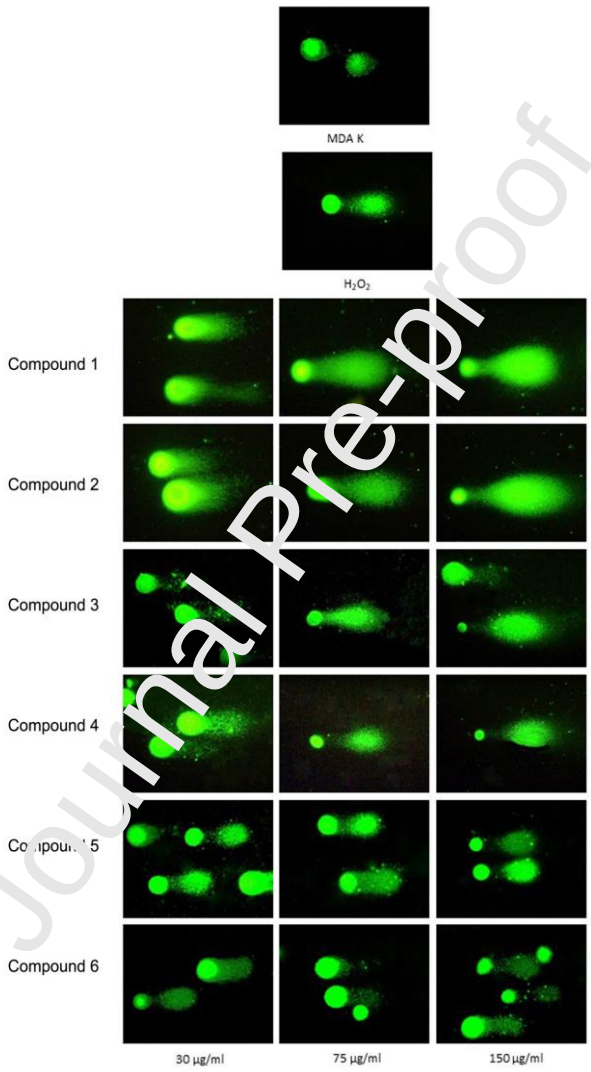

Figure 1: SCGE for testing the genotoxicity potential of quinazolin-4-one derivatives on MDA cells. Representative comet images of MDA cells incubated with increasing concentrations of all tested compounds (bar=10 µm).

Even though all substances exhibit significant level of genotoxicity with values of OTM above the green dotted line, **2**, **3** and **4** (Figure 2) indicate high levels of genotoxicity for the higher tested concentrations as seen on the micrographs on Figure 1. For compounds

1, **5**, **6** we detect weaker effect**,** that is, somewhat lower level of genotoxicity in comparison to the other tested quinazolin-4-one analogues.

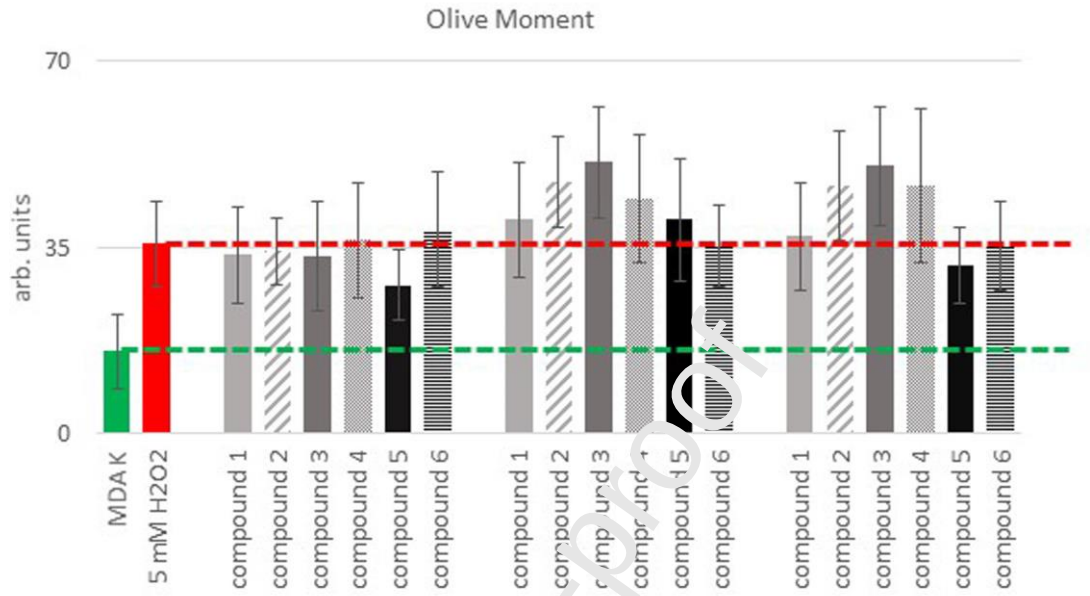

Figure 2: Graphical representation of the parameter "Olive Moment" (OTM) as quantified by the software CometScore. Data are represented as MEAN±STDV, where n=100. Additionally, the trendline in dotted green colour, approximately the 15 line, is showing the values of OTM for the healthy nuclei while the one in red (OTM at , arb. units) indicates that all values at and above it represent cell nuclei with damaged DNA. Left group is at heterocycle concentration 30 μg/ml; middle – at 75 μg/ml; and right – at 150 μg/ml.

2.2. *The tested compounds induce changes in the cellular morphology of MDA cells*

Following the results from the neutral SCGE and the clearly exhibited genotoxic potential of the tested substances on MDA cells we performed Fluorescence Activated Cell Sorting (FACS analysis) to study the molecular mechanism of action of the obtained genotoxicity. The first idea checked was whether tested quinazoline analogues have cytostatic effect which could potentially lead to accumulation of DNA damage and eventually to cell death. The results showed neither significant delay nor any change in the dynamics of cellular progression through the cell cycle phases in probes with and without treatment with the tested compounds (data not shown). Therefore, we further checked the cells for changes in their morphology as a possible consequence of the treatment.

FACS analysis allows relative estimation of changes in cellular morphology like changes in cellular size and, more important, intracellular granularity.[21] Results are shown on Figure 3. Data quantification has been done by measuring the forward scatter (FSC) and the side scatter (SSC). When measured in conjunction, these two measurements allow visualization of some degree of cellular differentiation within a heterogeneous population.[22] Graphs on Figure 3 show distribution of cells depending on their size and granularity. Three graphic representations are shown, giving the percentage of cells normal in size and granularity (Fig. 3A), cells normal in size but with high percentage of granularity (Fig. 3B) and cells with big size and high granularity (Fig. 3C). Generally, the heterogeneity of cells which differ in morphology is a characteristic of the process of malignization and is a good indicator for the action of potential anticancer agents.[23] We have detected the most explicit phenotype in cellular morphology of MDA cells after treatment with increasing concentrations of compounds **1** to **4.** In all tested concentrations the population of cells with normal size and normal granularity was low in comparison to the other populations (Fig. 3A). Notably, when we followed the distribution of cells with normal size but high granularity we have detected that the percentage of cells with high granularity was the highest after treatment of cells with compound **4** at all administered concentrations, Fig. 3B. The distribution of cells with big size and abnormal granularity proved most interesting, as seen from Fig. 3C. Treatment of MDA cells with compounds **5** and **6** led to accumulation of the highest percentage of cells with completely distorted morphology. This observation detects heterogeneity in the studied populations of cells and is a marker for some potential reorganization in cellular morphology which could be due to the applied treatment with the tested compounds. Generally, this idea needs further experiments in order to detect what exactly are these changes and whether they could be a marker for anticancer action of the studied quinazolin-4-one derivatives. As a matter of fact, all compounds **1 - 6** exhibited high genotoxic potential and also the ability to definitely change the cellular morphology of the cancer cells which determines these compounds as good candidates for further studies of their molecular mechanism of action on different cancer type cells. This might possibly require combination with other chemotherapeutics. Another potentially meaningful difference between **5** and **6,** and derivatives **1** to **4** is the reported activity of **6** on a topoisomerase,[24] dealing with DNA coiling completely different to telomerase, but nevertheless forming G-quadruplexes to, e.g., regulate transcription of oncogenes.[25]

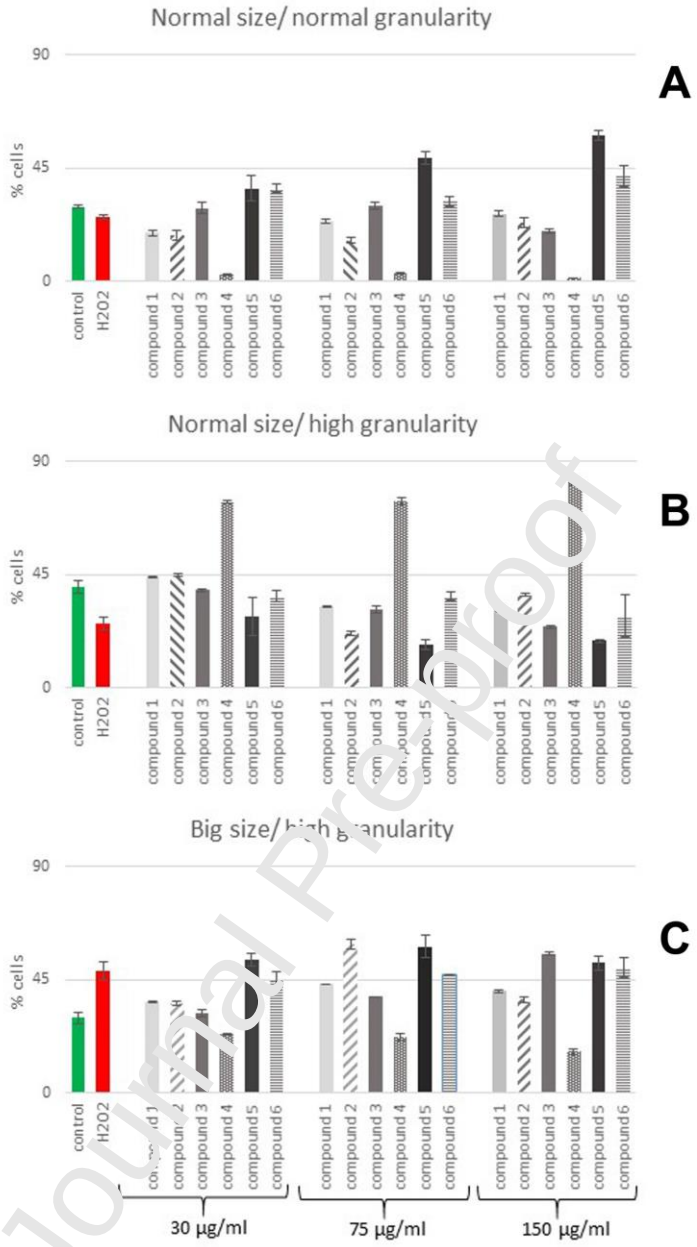

Figure 3: FACS analysis of MDA cells treated with 2-heterosubstituted quinazoline analogues **1** – **6,** see Scheme 1. Quantitation of FSC (forward scatter) *versus* SSC (side scatter).
A: Population of MDA cells with normal size and normal granularity
B: Population of MDA cells with normal size and high granularity
C: Population of MDA cells with big size and high granularity

The above experiments indicate unambiguously that the tested quinazoline analogues interact with DNA in the model cell cultures. The registered interactions may belong to several classes of small molecule interactions with NA helical structures, of which the outstanding ones are intercalation, groove binding, and selective targeting of specific

secondary sequences.[26] We start with the initial assumption of quinazoline intercalation into the helical ladder of DNA.[27] To check this by a physical experiment, we have used a buffer solution of DNA, in the presence of ethidium bromide label. Addition of compounds **5** and **6** le to the establishment of equilibrium between the intercalating fluorescence label and quinazoline analogue, see spectra in the Supporting information. Specifically, increasing concentration of the quinazoline analogue, **5** or **6**, in the solution reduce ethidium bromide fluorescence intensity proportionally by displacing the intercalator from DNA, the effect being more pronounced for **6**, which we interpret in terms of some intercalation, leading to displacement of ethidium from its DNA complex.

3. *Discussion and modeling*

3.1. *Mechanism of action*

So far, we have considered effects of structural variations of quinazoline analogues on their biological activity. To understand the reasons for the observed differences, we need to consider the interactions of studied molecules with their presumed biochemical counterparts. This is another more complicated level of molecular organization, which must include both studied heterocyclic molecules, and biological components. For this purpose, we attempt molecular dynamics simulation, MD, for the interactions of 2-substituted analogues of quinazoline with an arbitrary double-stranded GGGAAAGGG DNA oligomer.[28] Along the MD run, the free 3'-end of the GGG-fragment first opens its hydrogen bonds to their cytosine counterparts, giving the heterocyclic molecule the opportunity to insert into the momentarily split double helix. Then the helix self-repairs, keeping the intruder molecule between the first two base pairs, Fig. 4. MD results indicate that 2-heterocycle-substituted quinazoline analogues of approximately the size of NA base pairs, including **1** – **6**, are apparently capable to insert into free double stranded NA fragments.

However, neither the ethidium experiment, nor the MD result do necessarily suggest intercalation of quinazoline compounds into DNA and leaves open other modes of possible binding to DNA.[26] For example, binding of hydroxyl-rich antibiotic molecules[26] to one of DNA grooves is more likely a type of electrostatic interaction, which is not the case of studied heterocycles. There remain also possibilities of another type of stacking binding to DNA secondary structure beyond intercalation. The outlined dilemma has apparently been already solved by the suggestion of **6** binding to guanine quadruplexes.[24] The latter higher

order quadruple stranded NA structures form spontaneously in guanine-rich NA segments,[24,28] and actively regulate DNA self-expression.[29] Similar types of binding may take place with planar heterocyclic molecules, including naturally existing aromatic alkaloids,[12,25] and indeed with schizocommunin **3** as well.[7, 8] A significant amount of experimental work has been dedicated to the proof of G-quadruplex affinity to molecules with sufficiently extended π-electronic systems.

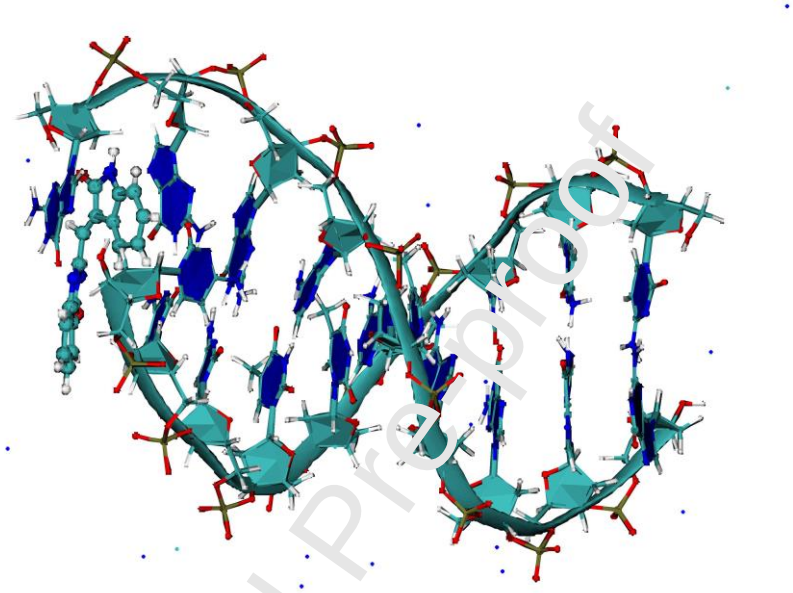

Figure 4: MD simulation of the insertion of **3** (on the left) into the ragged C3'-end of model DNA oligomer. Base pairs are shown in cyan, pentose in green pentagons and **3** in balls and bonds. Phosphate oxygen atoms are red, and scattered blue dots are random water molecules.

The results discussed so far suggest that direct intercalation of quinazolines into cell DNA is not the most likely mechanism of their biological activity, as far as the activity registered experimentally by us is only manifested on cells undergoing the complete cell cycle. An alternative is interaction of quinazoline analogues **1** – **6** with mentioned four-stranded NA structures, consisting of nucleotide quartets. Among the latter, guanine quartets and stacked structures thereof, G-quadruplexes, are the most abundant.[24, 25, 28, 33, 36] This type of interaction has been reported for **3**.[7, 8] For this very reason, schizocommunin **3** has evidently been considered a prospective pharmaceutical compound and has already ignited a series of sophisticated studies on its mechanism of action. The aim is obviously the understanding of future therapeutic prospects of this compound and its possible derivatives, as an opportunity to control stabilization of G-quadruplexes[7, 8] would mean opportunity to

influence their significant regulatory role(s) in DNA replication, transcription and expression in a broadest range of organisms, viruses, procaryotes, eukaryotes, and including humans, with rapidly reproducing cells. [29, 36, 37]

There is good probability that heterocycles would stack to guanine tetrads of telomeres as far as telomerase leaves the latter single-stranded ends free. The single strand DNA spontaneously self-associates into four-stranded helical DNA structures, comprised of several stacked guanine tetrads, usually stabilized by potassium, or sodium ions on top of each tetrad.[30, 33] The planar hydrogen bonded guanine quartets along with alkaline ions and pertaining sugar, nucleobase and phosphate moieties from connecting NA strands, form stacked G-quadruplexes,[30–36] which comprise an excellent site for additional interactions with external planar aromatic molecules. There is also a probability of additional G-quadruplex stabilization.[28,32,36] This stabilized spontaneous folding of single-stranded or temporarily split DNA into G-quadruplexes is considered a significant DNA damage, capable to disrupt normal telomerase (or other enzymes, e.g. topoisomerase[25]) function[8, 24] and leading eventually to apoptosis.

3.2. Experiments for G-quadruplex interactions with small molecules

The detailed structure of a telomeric 3'-terminal DNA quadruplex with daunomycin complex has been resolved by high resolution X-ray diffraction.[30] The quadruplex itself comprises four G-tetrad units, each stacked 3.35 Å apart, with a sodium cation coordinated between each pair of tetrads.[30] The complex structure is almost identical to the crystal structure of the native quadruplex.[30] In the crystal, two quadruplexes are stacked end-to-end, 5' to 5', the interface between the two being filled by two layers of daunomycin. No drug molecules are intercalated into the guanine core of the quadruplex.[30] The latter finding is supported also by NMR studies.[30 and references therein]

The affinity of human telomeric G-quadruplexes towards substituted quinazolines as highly selective ligands has been demonstrated using a number of spectroscopic methods. [31] These include fluorescence resonance energy transfer (FRET) DNA melting assay, circular dichroism (CD) spectroscopy, surface plasmon resonance and nuclear magnetic resonance, augmented by molecular docking. An essential result of this study is that unfused (aromatic nucleus) quinazolines are highly effective binding ligands.[31] Specifically, FRET

has been used to prove complex formation of telomeric G-quadruplex and ca. 30 schizocommunin **3** derivatives [8] and alcaloids.[12]

Another effective method for the study of ligand binding to G-quadruplex DNA is UV resonance Raman spectroscopy, [32] in addition to electronic absorption, emission, and circular dichroism spectra. Binding modes of two specifically designed dyes, BRACO19 and pyridostatin, have been compared to show the first been governed by π-π interactions, or "end-stacking", while the second conformationally very flexible molecule exhibits multiple binding modes.[32]

Circular dichroism and fluorescence spectroscopy have been used to show that two fused tetracyclic dye molecules bind to the 3'-terminal G-tetrad of a RNA polymerase promoter. The mentioned two tetracyclic dyes have strong antiproliferative effect on a human lymphoma model. The suggestion of a G-quadruplex binding mechanism has been supported also by NMR spectroscopy, molecular docking and molecular mechanics modelling. [33]

The reported types of small molecule binding to NA substructures are amenable to computational molecular modeling.[34-37] Our computational models would indeed aim at the structure and relation of computed physicochemical to experimental biological properties of DNA complexes with **1** – **6** and similar molecules in order to guide our understanding of their possible interference with the cell cycle. Our planar vinyl-substituted quinazolin-4-ones **1** and **2** are angularly fused pentacycles, while **3** and **4** are linearly fused pentacycles, Scheme 1, showing a hydrogen bonded quasiaromatic cycle in their middle, all potentially capable of π-π stacking.

3.3. *Modeling of quinazolin-4-one analogue interactions with G-quartets*

To model and quantify the stabilization of G-quartets due to their interactions with 2-substituted quinazolin-4-ones **1** – **6** we attempt direct electronic structure computation of the G-quartet itself, heterocyclic molecules, and the complexes thereof. The computations would also supply reliable spatial geometries of participating components and their changes due to formation of the corresponding complexes. For the latter, we derive acceptable starting geometries from molecular dynamics calculations, molecular graphics builders [39] and preliminary valence electron semiempirical MO calculations. [40] An important detail of

present computations is that G4-multiplex models are completely stripped off their pentose-phosphate backbone.

Current understanding of G-quartet structure, based on X-ray and NMR experiments, [30, 31] as well as MD simulations,[25, 34, 37] is of a square planar overall arrangement of atoms, apparently no more than an initial approximation. Wave function (or Molecular orbital) theory calculations, WFT, at the MP2/6-31G(d) [41] level show that the planar G-quartet is not a minimum in vacuum, Fig. 5, even though the potential energy surface is extremely flat, and distortions in the direction of shown twisted conformation require *ca.* 0.5 kcal.mol^{-1}. The located twisted minimum, with guanine planes at an angle of $30^{o} \pm 1^{o}$ of each other, is *ca.* 2 kcal.mol^{-1} lower. The small (≤ RT) vibrational distortions of the G-quartet in vacuum are further levelled down by SCS-MP2/6-31G(d) calculation, whereby the located minimum is visually almost planar. The rather strongly distorted minimum of a G-quartet resulting from calculations at the wB97XD/6-31+G(d,p) [42] level of density functional theory, DFT, is also shown on Fig. 5. Visually the M06-2x/6-31+G(d,p) geometry does not significantly differ from the wB97-XD/6-31+G(d,p) result. We find the association energy of four guanines into the Hoogsteen-type bound distorted square tetrad at ca. 75 kcal.mol^{-1}, predicted at the nonempirical electron correlated WFT level, SCS-MP2/6-31G(d,p) calculation in vacuum. The same association energy is ca. 82 kcal.mol^{-1}, optimized without the SCS correction. For the sake of comparison, Watson-Crick base pairing energies have been calculated by MP2/6-31G(d,p) to be in the range of 12 to 25 kcal.mol^{-1},[45] all values pertinent to in-plane interactions of NA bases. Finally, a DFT analysis of interaction energies in model NA quadruplets [43,44] shows that hydrogen bonding contributes ca. 50%, which refers to in-plane bonding of the four guanines. In principle, G-quadruplex calculations should also involve 3D interactions of layered bases, plus sugar and phosphate moieties as well. The present estimate is of 10 - 20% coming from stacking dispersion, [45] and assumes the remaining stabilization due to ion to base coordination energy.

Both experimental and theoretical G-quartet and layered quadruplex planar structural organizations, as mentioned above, comprise a convenient site to accommodate relatively large planar external molecules. In the case of aromatic ligands, like quinazoline analogues and larger heterocycles, the initial hydrogen-bonded G-quartet or stacked quadruplex complex would be additionally stabilized by π–electron dispersion stacking interactions. [30-32, 43, 44]

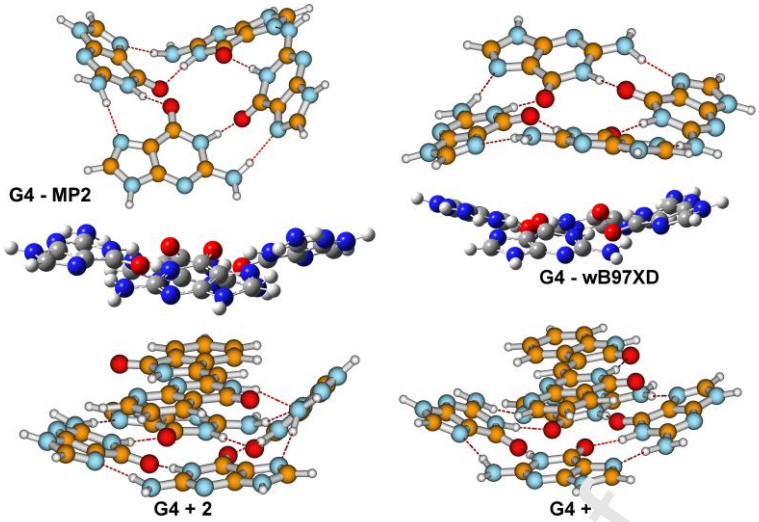

Figure 5: Optimized structures of a G-quartet, G4, and heterocyclic complexes in vacuum: top left, G4 at MP2/6-31G(d); top right – G4 at wB97XD/6-31+G(d,p). Bottom left: G4 + **2** complex, bottom right: G4 + **4** complex, both from wB97XD/6-31+G(d,p) calculations. Oxygen atoms are red, nitrogen atoms are blue and hydrogen bonds are represented by dotted lines.

SCS-MP2 calculations locate minimum energy arrangements of the complexes of a G-quartet and quinazoline analogues, the latter at approximately 34 pm of a somewhat puckered G-quartet ensemble, while the heterocyclic substituent approximately directed along its diagonal, isoindol-3-on-ylidene for **1** and **2**; indol-2-on-3-ylidene for **3** and **4**; 2-pyridyl for **5** and 2-quinolyl for **6**, the latter two possibly slightly tilted closer to edge guanine fragments, Fig. 6. The orientation of heterocyclic ligand is indeed dependent on its structure, which will be discussed in more detail below. DFT calculations of G-quartet complexes with substituted quinazoline analogues **1** – **6** in vacuum indicate somewhat stronger bending of bowl-like quartet forms in the complexes with respect to the isolated G-quartet. Accounting for the presence of solvent, using the traditional medium for physiological environment models, n-octanol, does not change this finding. The conformations of bowl-like G4 are essentially unchanged upon complexation with **2** and **4**, Fig. 5, and indicate a minor role of heterocyclic ligand structure on the conformation of its G-quartet complex. Evidently the mentioned molecular shapes depend on known types [43 – 47] of interactions between NA base pairs and stacked ligands, in this case between a G-quartet and substituted quinazoline analogues.

Recent detailed studies of NA pair stacking interactions indicate that dispersion covers 70 to 85% of the total interaction energy,[35] expected to be quantitatively correctly reproduced[44-46] by MP2 or, better, SCS-MP2[41] calculations. The still significant electrostatic contribution to base stacking energies is responsible for 10 – 20% of the latter. [34] Another feature worth mentioning of these calculations is the indication of possible hydrogen bonding between the G-quartet and quinazolin-4-one analogues, see complexes with **2** and **4** on Fig. 5, increasing the stabilization in addition to dispersion interactions. In the present case of a G-quartet stacking with a single extended nitrogen base among **1** – **6** we guess that electrostatic interactions in the form of additional out of plane hydrogen bonds might contribute up to 25% of the interaction energy, see DFT structures on Figure 5. On the other hand, we are currently not in the position to analyze precisely the contribution of the mentioned two components of interaction energy, requiring sufficiently flexible basis sets in either DFT or even less SCS-MP2 calculations of G-quartet complexes.

Table 1: Total stabilization energies of the G-quartet, stacked with quinazoline analogues, DFT and SCS-MP2 in vacuum. Stabilization ΔΔE, in kcal.mol^{-1}, is given as positive.

Heterocyclic ligand	wB97XD/ 6-31+G(d,p)	M06-2x/ 6-31+G(d,p)	SCS-MP2/ 6-31G
1	36.0	30.7	23.6
2	32.6	28.7	21.1
3	31.6	31.2	18.1
4	31.8	30.0	18.8
5	27.0	23.1	26.8
6	34.4	27.3	19.7

The most important feature we are looking for is whether the computed stabilization energies of G-quartet complexes correlate with activities of compounds **1** – **6**, determined by experiments in *Section 2*. Table 1 does not show the expected correlation of calculated G-quartet stabilization energies upon interaction with heterocycles **1 – 6**, against our experimental biological activity results. Both wB97XD and M06-2x results seem rather chaotic. The same is true for the MP2 electron correlated calculations. We therefore consider some computed interaction energies of G-quartet and heterocyclic quinazoline-like ligands in terms of more structural detail. As might be expected, within the selected set of six

compounds or, better, three pairs of very close analogues, see Scheme 1, calculated stabilizations of G-quartet ligand complexes also form three pairs of values. In the pair **1 – 2** the latter more biologically active compound should show at least stronger stabilization by the dispersion corrected wB97XD calculations, which is not confirmed in Table 1 by either method. For the **3** – **4** pair, experiment shows higher activity for **4**, Fig. 2B, while computed interaction energies are inconclusive. In the pair **5** – **6,** our observed order of activities is correctly reproduced by calculated DFT interaction energies but not by MP2 results. Computed differences of G-quartet interaction energies within pairs of ligands may be associated with changes of dispersion energy due to changes of quinazoline to pyrido[2,3-d] pyrimidine fragments in the first two pairs. Unclear remains why the MP2 result for **5** vs. **6** does not reflect the expected stronger π-dispersion interaction with the quinoline heterocycle, compared to pyridine, see Fig. 6, while DFT results are at least in agreement with our experimental observations.

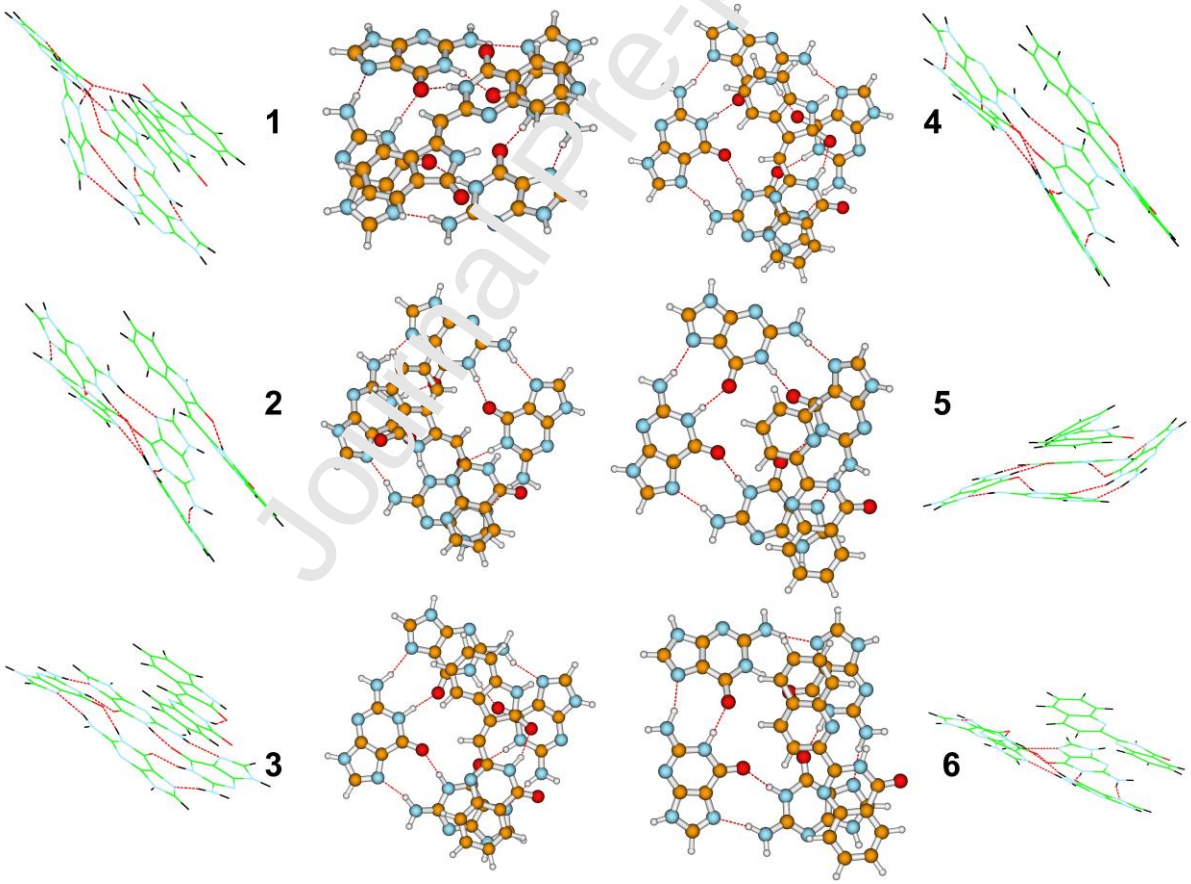

Figure 6: SCS-MP2/6-31G [41, 48] optimized structures of G-quartet complexes with heterocyclic ligands **1** – **6**. Interaction energies are listed in Table 1. Nitrogen atoms are blue, oxygen atoms – red, and hydrogen bonds are given with dotted lines. Distances between ligands and approximate planes of G-quartets in **2** – **4,** or from "chair" to ligand in the chair-like conformations of **1**, **5** and **6**, are 35 to 40 pm.

Examining Fig. 6, one notices that there should be at least two reasons for the absence of correlation between computed stabilization energies of G-quartet – heterocyclic complexes, and observed biological activity in this work. As mentioned above, the first reason would be the structural flexibility of π-electron-defined dispersion dominated complexes, which would prefer quasi-parallel arrangement of ligands and G-quartet, even though π-electron dispersion interactions may or may not dominate the overall stacking interaction energy. The DFT conformational predictions of complexes are more clearly dominated by the second type of interactions – electrostatic, wrapping the G4 around the heterocyclic ligand, Figure 5. Additionally, a ligand may also form out-of-plane hydrogen bonds with the G-quartet, which may significantly distort the parallel arrangement of bases and alter the overall stabilization energy by 15 – 20%, see Figure 6, complex 1. This energy estimate comes from the comparison of energies of a single hydrogen bond, *ca*. 5 kcal.mol^{-1}, and calculated stacking energies of heterocycles to a G-quartet, *ca*. 30 kcal.mol^{-1}, Table 1. Another reason for the absence of linearity between G-quartet complex stabilization and observed biological activity might arise from differences in targeting of G-quartets by corresponding heterocyclic ligands: quasi-symmetrical ligand positioning along the quartet diagonal, found for **1** – **4**, or unsymmetrical position of the ligand along an edge of the G-quartet as **5** and **6**, see Figure 6. The flexibility of single G-quartets however seems the main reason they offer no good approximation to interaction energies of ligand complexes with G-quadruplexes. One could safely suggest that quadruplex aggregates would be considerably more rigid than single guanine quartets.

One more reason for the apparently complicated relationship between G-quartet – ligand stabilization and the observed activities might result from differences between G-quadruplex regulated apparitions of DNA. Regulation or retardation of different G-quadruplex dependent enzymes might also require different alignment of G-quadruplex and heterocyclic ligand, and even different constitution of the quadruplex with two stacked G-tetrads instead of three, as reported in the case of human topoisomerase 1,[25] see Figure 7. Another possible cooperative effect of stacked G-quadruplexes, with their constitutively belonging alkaline metal ions, would stem from their additional electrostatic and ion coordination stabilization.

3.4. *Modeling of quinazolin-4-one analogue interactions with G-quadruplexes*

Therefore, we attempt to compute the stabilization of a more extended model, a G-quadruplex, consisting of two or three stacked guanine tetrads internally stabilized by

potassium cations, and the heterocycle stacked to the bottom guanine tetrad. DFT calculation results with both selected functionals in Table 2 on quinazoline analogues **1** – **6** relatively closely mimic the results of biological experiments reported in *Section 2*. The smooth increasing of stabilization by interactions energies of G-quadruplex and heterocycles **1** – **4** is intuitively very satisfying to the chemical common sense, as is to some extent the ordering of the corresponding values for heterocycles **5** and **6**, Figs. 2 and 3.

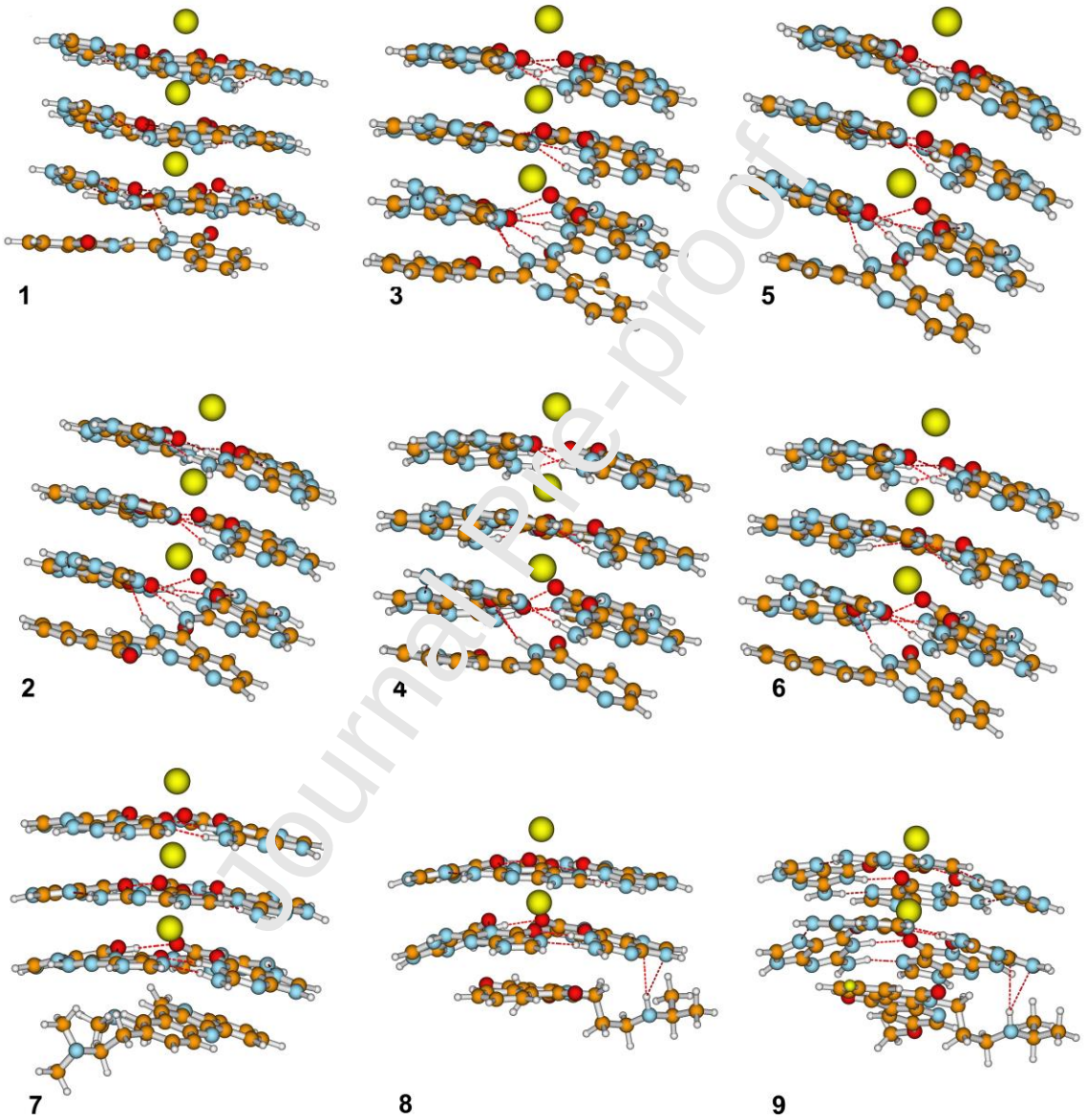

Figure 7: Heterocyclic ligands **1 – 7** stacked to the bottom of telomeric $3K^+$.G-quaruplex model. Nitrogen atoms are blue, oxygen atoms are red, and potassium atoms are gold. Hydrogen bonds appear as dashed lines in G-quartet planes, as well as between the bottom quartet and the heterocyclic ligand. Complexes of **8** and **9** with two-layered G-quadruplex, reported for topoisomerase 1 [25] are shown as well. G-quartets in the latter two-layered quadruplexes have visibly stronger-bent bowl conformations. Fluorine in the plane of heterocycle **9** is yellow. Possible hydrogen bonds of side chains and bottom quadruplet are visible as well, **8** and **9**.

3.5. *Modeling and quantitative structure relationships*

It would be interesting to include some additional heterocycles known for their useful anticancer activity in the same interaction model. Therefore, we list in Table 2 also the results on models of G4 quadruplex interactions of heterocycles **7**, a quindoline alkaloid with known G-quadruplex from NMR; [12, 24, 53] indeno-isoquinolines **8** and **9 [**25]; and **10**, another natural quinazoline alkaloid, luotonin.[24] There is also the benzo[b]naphtho[2,3-d]furan tetracycle **11**, which is not a nitrogen base, but is a telomerase inhibitor on its own right, Scheme 2. [25, 54, 55]

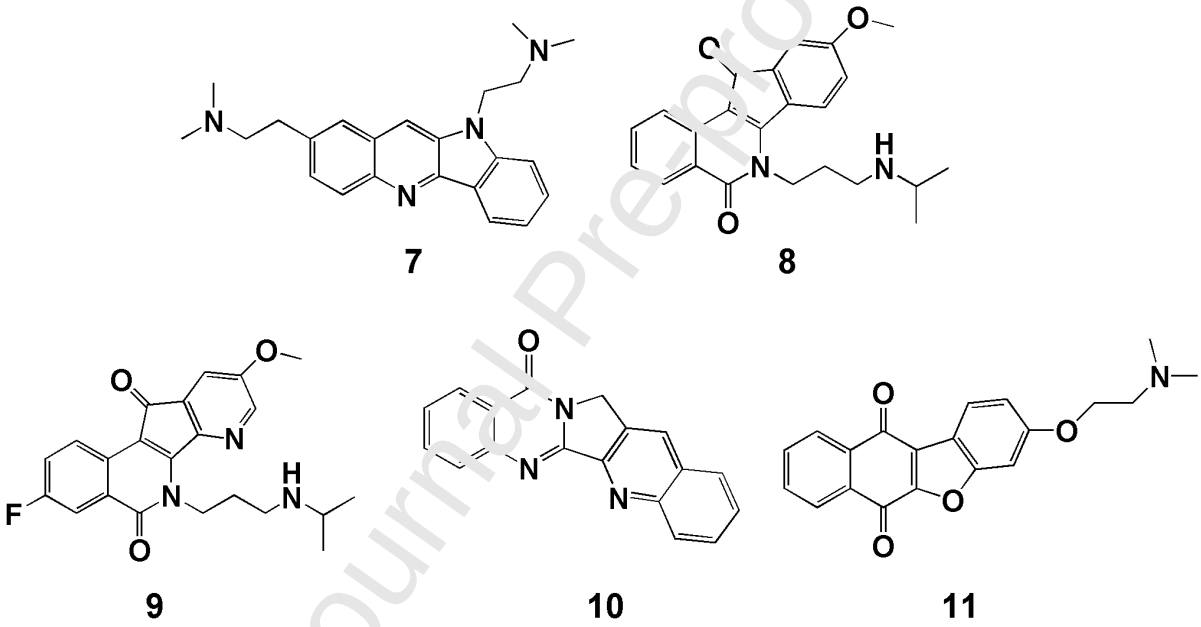

Scheme 2: A quindoline derivative **7**, [12, 24, 53] and an electron-acceptor, naphtho[2,3-d] benzo[b] furan tetracycle **11**, [54] acting as telomerase inhibitors; [12,54,55] two indeno-isoquinolines **8** and **9**, [25] and the quinazoline-4-one alkaloid **10**, luotonin A, [24] acting as potent anticancer agents by specifically suppressing transcriptional activity of topoisomerase 1.

It is satisfying to note, that use of quantum chemical models corroborates the hypothesis of G-quadruplex – ligand stabilization governing anticancer activity of heterocyclic compounds.[53-55] The main indication from computed wB97XD/6-31G(d,p) and M06-2x/6-31G(d) interaction energies of heterocycles with the model potassium ion G-

quadruplexes is that possible anticancer activity of quinazoline analogues **1 – 4** should be expected to be comparable to quantitatively established activity of quindoline **7**,[53] as well as naphtho-benzofuran **11**, [54] but perhaps lower than registered high activity of indeno-isoquinoline **9**. [25] A comparison between lower 6-31G(d), Tables 3S and 4S, and higher 6-31G(d,p) basis set calculations, Table 2 here, shows that the more flexible basis set gives a crisper numerical presentation of the chemical common sense discussion, while somewhat increasing hydrogen bonding between bottom guanine tetrad and stacked ligand, see Fig. 7.

Table 2: Stabilization energies ΔΔE, kcal.mol^{-1}, of heterocyclic ligand complexes with **G4** quadruplexes with potassium cations, calculated at the 6-31G(d,p) level in vacuum. [48,49] Model three-layered G-quadruplex Q4.3K$^+$, related to telomerase inhibitors, or two-layered Q2.2K$^+$ model, reported for topoisomerase 1, [25] is used for with heterocycles **8,** and **9;** data shown in italics**.** For **5, 6,** and **10** we give the results for both models.

	M06-2x/6-31G(d)	**wB97-XD/ 6-31G(d.p)**	**RIMP2/6-31G(d,p)/ SVP // wB97XD/ 6-31G(d,p)**
Heterocyclic Ligand	**ΔE_0, kcal.mol^{-1}**	**ΔE_0, kcal.mol^{-1}**	**ΔE_0, kcal.mol^{-1}**
1	**37.41**	**42.70**	**53.81**
2	**39.52**	**43.35**	**47.89**
3	**51.82**	**44.10**	**49.05**
4	**40.77**	**43.77**	**48.75**
5	**20.21** ***26.03***	**26.19** ***25.29***	**32.69** ***30.79***
6	**36.50** ***28.17***	**29.72** ***28.99***	**47.81** ***34.76***
7[53]	**41.73**	**46.70**	**50.11**
8[25]	***39.89***	***44.29***	***49.20***
9[25]	***45.29***	***47.48***	***58.52***
10[24]	**37.09** ***36.41***	**36.79** ***36.86***	**42.95** ***42.64***
11[54]	**35.59**	**46.40**	**52.31**

To refine and analyze the DFT results at a higher level theoretical detail, we need an efficient methodology to obtain more reliable approximations to the components of interaction energies within layered G-quadruplexes themselves, as well of their interactions with potentially stabilizing external heterocycles of the kind discussed so far in the present paper. As far as stacking models are concerned, quantitatively more reliable dispersion energies might only be obtained by, for example, selected computationally efficient dispersion-corrected DFT methods,[42-44] or higher level CCSD or CCSD(T) calculations, using sufficiently flexible basis sets in either case. With the large number of atoms and electrons in the model G-quadruplex – nitrogen base complexes studied here, up to 250 atoms and 600 occupied orbitals, the indicated electron correlated computations would be indeed prohibitively expensive. However, the necessary methodology does exist in the form of resolution-of-the-identity, RI, approximation, [56] and has been specifically designed to overcome the massive resource requirements of explicit complete electron correlated computations. We use the optimized wB97XD/6-31G(d,p) geometries of G-quadruplex – heterocycle complexes to carry out single point resolution of identity RI-MP2/6-31G(d,p)/ SVP calculations. The obtained results are listed in Table 2 as well, and complete details may be found as Table 5S of the Supporting information.

Stabilization energies of G-quadruplex complexes with heterocycles with quantitatively measured inhibition effects on telomerase, **7** and **11**,[53] and topoisomerase 1, **8** and **9**, [25] from Table 2 are comparable to the calculated values for quinazoline analogues **1** – **4**. This result shows once again that expected anticancer activity of **1** – **4** should at least be moderate or, for derivatives of **3**, [8] comparable to that of the electron-acceptor tetracycle **11. [**54] Activities of **5** and **6** should be obviously lower than the activity of indeno-isoquinolines **8** and **9. [**25] There is however a more important indication given by the found correlation between calculated stabilization energies of G-quadruplex complexes with heterocycles: the used model of planar heterocycles stacking to the bottom G-tetrad in NA guanine quadruplexes is probably close enough to reality. A similar correlation has been reported for results of molecular mechanics modelling of G-quartet heterocyclic complexes and their telomerase inhibitor activities.[34, 53-55] Further studies of detailed conformational and other structural effects within G-quadruplex complexes with heterocyclic ligands by quantum chemical computations are in progress.

4. *Conclusions and Outlook*

Anticancer activity exhibited by natural alkaloids and synthetic heterocycles, including quinazoline analogues, may in a number of cases be due to their contribution to the stabilization of four-stranded G-quadruplexes, observed in guanine-rich NA sequences. This work uses a model of G-quadruplex stabilization by heterocyclic molecules stacking to its bottom. On the basis of this model, and without preliminary expectations of possible activity and/or biochemical mechanism, we find correlations of observed biological response and computed stabilization energies. The stabilization of G-quadruplex models by heterocycles may thus serve as a convenient screening tool for anticancer compounds. The correlation revealed between biological response and computed model interaction energy may evidently serve also the opposite goal, namely, if a physical computational model predicts interaction energies of participating biological components with observed effects, then there is significant probability that the hypothesized model of their interaction correctly reproduces the real mechanism eliciting the observed response.

Ligands offering sites for intra- and intermolecular hydrogen bonding including possibilities for tautomerization may also be screened computationally for their respective interaction energies and physico-chemical properties by the suggested approach. Important is that more than half of the numerous publications on G-quadruplexes are concerned with various types of cancer,[54, 55] and the computational all-electron DFT approach offers significant promise to their understanding and to the search for novel drugs. Moreover, the outlined DFT computational procedure has significant reserves in terms of expanding the size of molecular models in general and might thus be a useful contribution to the host of *in silico* approaches [35, 57 – 59] in the search of novel G-quadruplex binding compounds, and vice versa, corroborates or may possibly oppose participation of G-quadruplex interactions in the biochemical mechanism in question. Moreover, a broader spread of anticancer and antiviral preparations based on G-quadruplex interactions may be of increasing use in medicinal practice. [55, 60]

5. Materials and Methods

5.1. Chemistry of 2-substituted quinazolin-4-one analogues

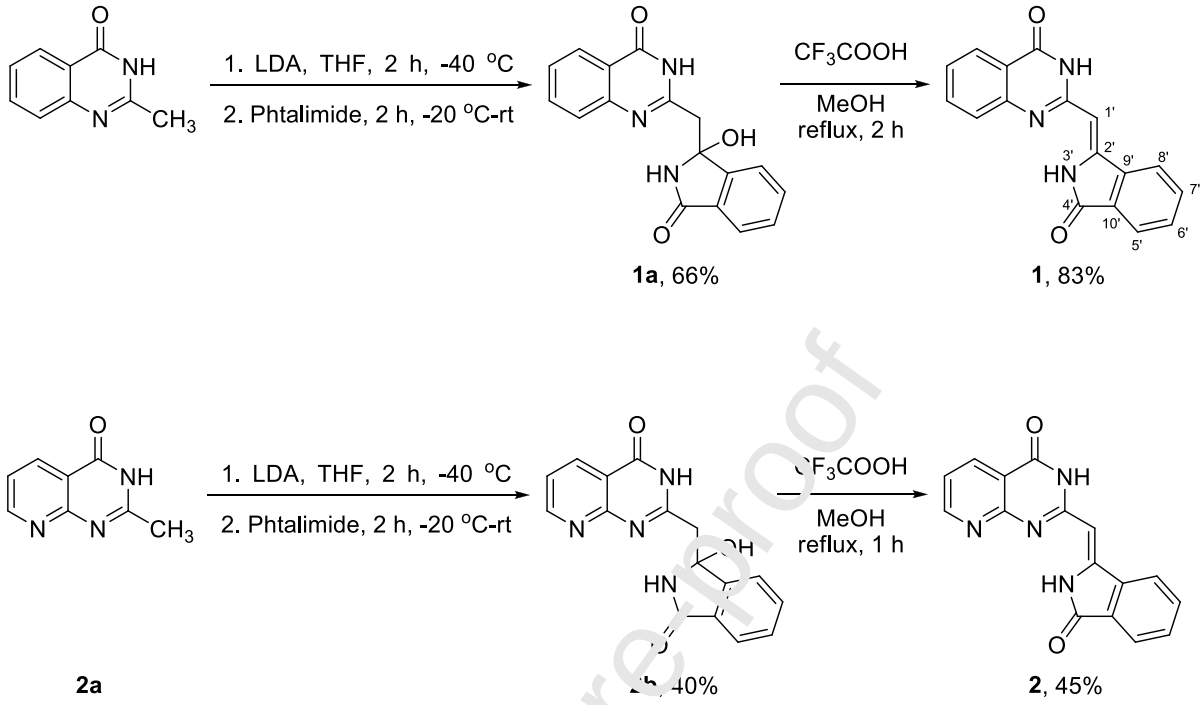

Scheme 3: Synthesis of compounds **1** and **2**. Numbering of heterocyclic rings corresponds to that of the ^{1}H and ^{13}C NMR spectra.

An efficient two step aldol type synthesis of 2-substituted-quinazolinones involves double lithiation of 2-methyl-3(3*H*)-quinazolin-4-one and subsequent *in situ* trapping with variety of electrophiles.[1S] The same approach is applied for the preparation of 2-((3-oxoisoindolin-1-ylidene)methyl)quinazolin-4(3*H*)-one **1** (Scheme 1S). Thus, lithiation of 2-methyl-quinazolin-4-one with 3 equivalents of LDA in THF at -78 °C followed by addition of phthalimide furnished the key intermediate **1a** in 66% yield. The latter was subsequently dehydrated with trifluoroacetic acid in refluxing methanol. The targeted 2-substituted-4(3*H*)-quinazolinone **1** was obtained in 83% yield after recrystallization from methanol, pale yellow powder. The structure was confirmed by H and C NMR.

Applying the same protocol for 2-methylpyrido[2,3-d]pyrimidin-4(3*H*)-one **2a** we synthesized the corresponding (*Z*)-2-((3-oxoisoindolin-1-ylidene)methyl)pyrido[2,3-d] pyrimidin-4(3*H*)-one **2** (Scheme 1S). The starting compound **2a** was synthesized from commercially available 2-aminonicotinic acid in a two-step procedure in analogy to the reported method.[2S] The key intermediate **2b** was obtained in 40% yield and used immediately

in the next step without purification because when exposed to the air for a few hours decomposition back to the starting compound **2a** occurred. The targeted **2** was obtained by dehydration with trifluoroacetic acid in refluxing methanol. The product was isolated in 45% yield after recrystallization from methanol, pale yellow powder.

Another aldol type synthesis has been reported for the natural schizocommunin **3** (Scheme 2S). Initially, the reaction of commercially available 2-methylquinazolin-4(3*H*)-one with isatin (indoline-2,3-dione) in refluxing acetic acid provided (*Z*)-2-((2′-oxoindolin-3′-ylidene) methyl)quinazolin-4(3*H*)-one (schizocommunin) **3** isolated in 64% yield.[3S] In an analogous fashion starting from 2-methylpyrido[2,3-d]pyrimidin-4(3*H*)-one **2a** we synthesized the corresponding (*Z*)-2-((2-oxoindolin-3-ylidene)methyl)pyrido[2,3-d] pyrimidin-4(3*H*)-one **4**. The reaction proceeded much faster and product was obtained in 86% yields within 1 h.

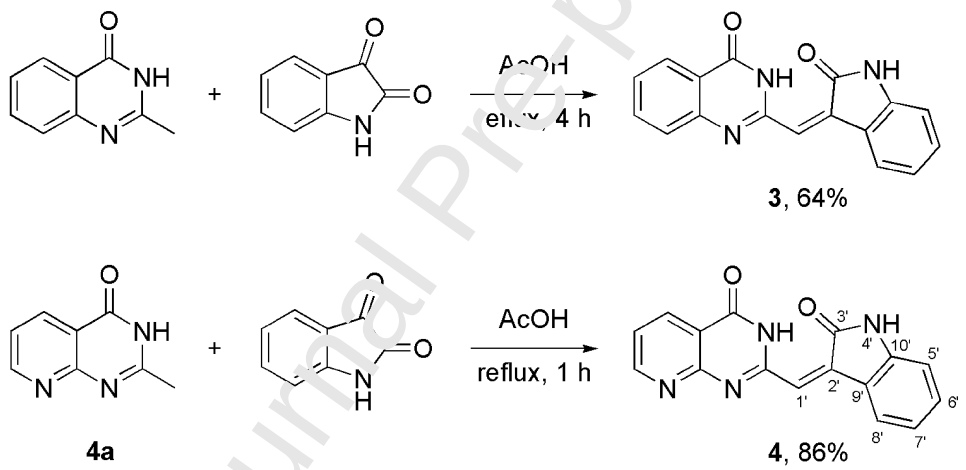

Scheme 4: Synthesis of compounds **3** and **4**. Numbering of heterocyclic rings corresponds to that of the ^{1}H and ^{13}C NMR- spectra.

The synthesis of the target 2-substituted-quinazolinone derivatives **5** and **6** was accomplished in one pot procedure *via* cyclization of 2-aminobenzamide with aldehydes in the presence of iodine as oxidant (Scheme 3S). The addition of catalytic amount of *p*-toluenesulfonic acid was crucial for the success of the condensation step. Thus, the reaction of 2-aminobenzamide with pyridine-2-carbaldehyde in THF led to the formation of 2-(pyridin-2-yl)quinazolin-4(3*H*)-one **5**, isolated in 72% yield after recrystallization from CH_3OH. Following the same protocol with quinoline-2-carboxaldehyde we synthesized the corresponding 2-(quinoline-2-yl)quinazolin-4(3*H*)-one **6** in 61% yield.

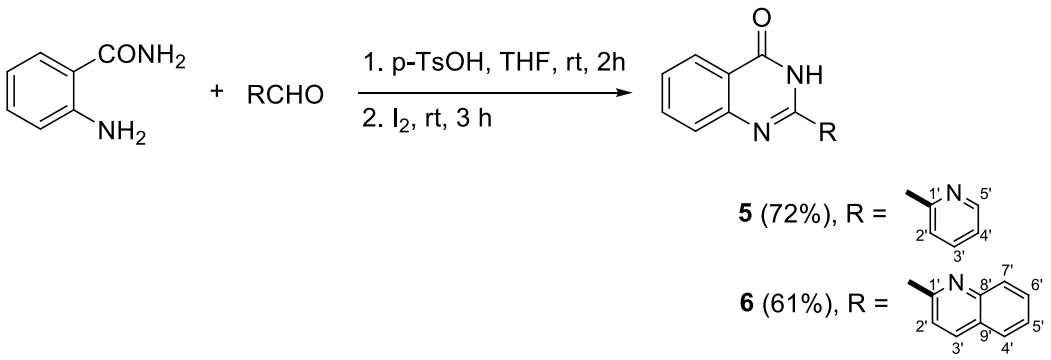

Scheme 5: Synthesis of compounds **5** and **6**. Numbering of heterocyclic rings corresponds to that of the ^{1}H and ^{13}C NMR spectra.

5.2 Synthesis of 2-substituted quinazolin-4-one analoguesReagents were commercial grade and used without further purification. Thin-layer chromatography (TLC) was performed on aluminium sheets precoated with Merck Kieselgel 60 F254 0.25 mm (Merck). Flash-column chromatography was carried out using Silica Gel 60 230–400 mesh (Fluka). Commercially available solvents were used for reactions, TLC, and column chromatography. The NMR spectra were recorded on a Bruker Avance II+ 600 (600.13 for ^{1}H MHz and 150.92 MHz for ^{13}C NMR) spectrometer with TMS as internal standards for chemical shifts (δ, ppm). ^{1}H and ^{13}C NMR data are reported as follows: chemical shift, multiplicity (s = singlet, d = doublet, t = triplet, q = quartet, br = broad, m = multiplet), coupling constants (Hz), integration and identification. The assignment of the ^{1}H and ^{13}C NMR spectra was made on the basis of COSY and HSQC experiments. The melting points were determined in capillary tubes on SRS MPA100 OptiMelt (Sunnyvale, CA, USA) automated melting point system with the heating rate set at 1° C/min. Elemental analyses were performed by Micro analytical service Laboratory of the Institute of Organic Chemistry, Bulgarian Academy of Science.

5.2.1 *Synthesis of 2-((1-hydroxy-3-oxoisoindolin-1-yl)methyl)quinazolin-4(3H)-one* ***1a****.*

A 2M solution of LDA in THF/*n*-hexane (1.50 ml, 3 mmol) was added dropwise to a stirred solution of 2-methyl-quinazolin-4-one (0.160 g, 1 mmol) in anhydrous THF (15 ml) at -78°C under argon atmosphere. Formation of the dianion was observed as a very deep red solution. The mixture was stirred at -78 °C for 2 h, after which phtalimide (0.176 g, 1.2 mmol) was added. The mixture was stirred for 2 h, then removed from the cooling bath and allowed to warm to room temperature and subsequently neutralized with saturated aqueous ammonium chloride solution. The mixture was extracted with dichloromethane, dried over

Na_2SO_4, filtered and concentrated to give crude product. Recrystallization from methanol gave 0.204 g (66%) of **6** as a light yellow solid. ^{1}H NMR: (DMSO-d_6, 600 MHz): δ 11.95 (br, 1H, NH), 8.84 (s, 1H, NH), 8.05 (d, *J* = 7.3 Hz, 1H, H-5), 7.75 (dt, *J* = 7.7, 1.1 Hz, 1H, H-7), 7.63-7.59 (m, 2H, H-5', H-6'), 7.55 (d, *J* = 7.4 Hz, 1H, H-8'), 7.52 (d, *J* = 8.2 Hz, 1H, H-8), 7.49-7.44 (m, 2H, H-6, H-7'), 6.81 (br, 1H, OH), 3.42-3.39 (m, 1H, H-1'), 3.15 (d, *J* = 13.9 Hz, 1H, H-1') ppm. ^{13}C NMR: (DMSO-d_6, 150.9 MHz): δ 168.02 (CO), 161.88 (CO), 153.41 (C-2), 148.86 (C-9, C-9'), 134.77 (C-7), 132.58 (C-6'), 131.76 (C-10'), 129.78 (C-7'), 127.38 (C-5'), 126.75 (C-6), 126.07 (C-5), 123.15 (C-8'), 122.86 (C-8), 121.37 (C-10), 88.54 (C-2'), 44.10 (C-1') ppm.

5.2.2 *Synthesis of 2-((3-oxoisoindolin-1-ylidene)methyl)quinazolin-4(3H)-one* **1**.

To a solution of **1a** (0.145 g, 0.469 mmol) in methanol (18 ml) was added trifluoroacetic acid (3 ml) and the reaction mixture was stirred under reflux for 2h. The mixture was neutralized with aqueous saturated sodium bicarbonate solution and the obtained precipitate was filtered off and recrystallized from methanol to give 0.109 g (83%) of **7** as an orange solid. ^{1}H NMR: (DMSO-d_6, 600 MHz): δ 12.42 (br, 1H, NH), 11.10 (s, 1H, NH), 8.08 (d, *J* = 7.6 Hz, 1H, H-5), 7.98 (d, *J* = 7.6 Hz, 1H, H-5'), 7.88-7.85 (m, 2H, H-8, H-8'), 7.82-7.78 (m, 2H, H-7, H-6'), 7.69 (t, *J* = 7.2 Hz, 1H, H-7'), 7.47 (t, *J* = 7.3 Hz, 1H, H-6), 6.33 (s, 1H, H-1') ppm. ^{13}C NMR: (DMSO-d_6, 150.9 MHz): δ 168.01 (CO), 161.58 (CO), 151.92 (C-2), 148.77 (C-9), 142.77 (C-2'), 136.73 (C-10'), 134.66 (C-7), 133.44 (C-6'), 131.51 (C-7'), 128.73 (C-9'), 127.43 (C-5'), 126.45 (C-6), 125.81 (C-5), 123.70 (C-8'), 121.06 (C-8), 120.45 (C-10), 94.19 (C-1') ppm; m.p. 350.2-350.6 °C. $C_{17}H_{11}N_3O_2$ (289.29): calcd. C 70.58, H 3.83, N 14.53, found C 70.73, H 3.62, N 14.60.

5.2.3 *Synthesis of (Z)-2-((3-oxoisoindolin-1-ylidene)methyl)pyrido[2,3-d] pyrimidin-4(3H)-one* ***2***.

A 2M solution of LDA in THF/*n*-hexane (1.50 ml, 3 mmol) was added dropwise to a stirred solution of **2a** (0.161 g, 1 mmol) in anhydrous THF (15 ml) at -78°C under argon atmosphere. Formation of the dianion was observed as a very deep red solution. The mixture was stirred at -78 °C for 2 h, after which phtalimide (0.160 g, 1.1 mmol) was added. The mixture was stirred for 2 h, then removed from the cooling bath and allowed to warm to room temperature and subsequently neutralized with aqueous saturated ammonium chloride solution. The mixture was extracted with dichloromethane, dried over Na_2SO_4, filtered and concentrated to give 0.124 g (40%) of crude **2b** as a white solid. To a solution of **2b** (0.124 g, 0.402 mmol) in methanol (12 ml) was added trifluoroacetic acid (3.5 ml) and the reaction mixture was stirred under reflux for 1h. The mixture was neutralized with aqueous saturated

sodium bicarbonate solution and the obtained precipitate was filtered off and recrystallized from methanol to give 0.079 g (45%) of **2** as an yellow solid. ^{1}H NMR: ($CDCl_3$/CF_3CO_2H, 600 MHz): δ 9.30 (d, *J* = 6.1 Hz, 1H, H-7), 8.86 (br, 1H, H-5), 8.02 (d, *J* = 7.3 Hz, 1H, H-5'), 7.97-7.96 (m, 2H, H-6, H-8'), 7.87 (t, *J* = 7.3 Hz, 1H, H-6'), 7.81 (t, *J* = 7.4 Hz, 1H, H-7'), 6.41 (s, 1H, H-1') ppm. ^{13}C NMR: ($CDCl_3$/CF_3CO_2H, 150.9 MHz): δ 169.94 (CO), 163.00 (CO), 159.94 (C-9), 156.18 (C-2), 151.36 (C-2'), 147.81 (C-7), 146.45 (C-5), 135.41 (C-6'), 135.16 (C-9'), 133.77 (C-7'), 127.95 (C-10'), 125.34 (C-5'), 122.60 (C-6), 122.43 (C-8'), 120.92 (C-10), 93.54 (C-1') ppm; m. p. 356.2-356.5 °C. $C_{16}H_{10}N_4O_2$ (290.28): calcd. C 66.20, H 3.47, N 19.30, found C 66.40, H 3.58, N 19.55.

5.3 Synthesis of compounds 3 and 4

A mixture of 2-methyl-4(3*H*)-quinazolinone or 2-methylpyrido[2,3-d]pyrimidin-4(3*H*)-one **2a** (1.0 mmol; 1.0 equiv.) and isatin (1.2 mmol, 1.2 equiv.) in glacial acetic acid (5 ml) were refluxed for 1 to 4 hours. After the mixture was allowed to cool to room temperature, the precipitate was filtered, washed with water and methanol, then dried to afford pure product.

*5.3.1 (Z)-2-((2'-Oxoindolin-3'-ylidene)methyl)quinazolin-4(3H)-one (**3**)*

Following the literature procedure, compound **3** was obtained as a yellow solid, yield: 64%. The spectroscopic data were in good agreement with the literature [*J. Nat. Prod.* **2013**, *76*, 2034−2039]. ^{1}H NMR: (DMSO-d_6, 600 MHz): δ 14.40 (br, 1H, NH), 11.50 (br, 1H, NH), 8.17 (d, *J* = 7.7 Hz, 1H, H-5), 7.94 (d, *J* = 7.4 Hz, 1H, H-8), 7.88 (t, *J* = 7.4 Hz, 1H, H-7), 7.78 (d, *J* = 8.0 Hz, 1H, H-6'), 7.60 (t, *J* = 7.7 Hz, 1H, H-6), 7.57 (s, 1H, H-1'), 7.36 (t, *J* = 7.5 Hz, 1H, H-6'), 7.08 (t, *J* = 7.4 Hz, 1H, H-7'), 6.93 (d, *J* = 7.6 Hz, 1H, H-5') ppm; m. p. 283.6-283.9 °C (lit.[2S] 284-286 °C). $C_{17}H_{11}N_3O_2$ (289.29): calcd. C 70.58, H 3.83, N 14.53, found C 70.26, H 3.98, N 14.75.

*5.3.2 (Z)-2-((2-oxoindolin-3-ylidene)methyl)pyrido[2,3-d]pyrimidin-4(3H)-one (**4**)*

Following general procedure, compound **4** was obtained as a red solid, yield, 86%. ^{1}H NMR: ($CDCl_3$/CF_3CO_2H, 600 MHz): δ 9.42 (br, 1H, NH), 9.33 (d, *J* = 7.7 Hz, 1H, H-7), 9.20 (d, *J* = 5.2 Hz, 1H, H-5), 8.04 (dt, *J* = 7.7 Hz, 1H, H-6), 7.74 (d, *J* = 7.7 Hz, 1H, H-8'), 7.52 (t, *J* = 7.7 Hz, 1H, H-6'), 7.49 (s, 1H, H-1'), 7.27 (t, *J* = 7.5 Hz, 1H, H-7'), 7.07 (d, *J* = 7.6 Hz, 1H, H-5') ppm. ^{13}C NMR: ($CDCl_3$/CF_3CO_2H, 150.9 MHz): δ 169.64 (CO), 160.00 (CO), 157.40 (C-8, C-2'), 152.86 (C-1'), 148.63 (C-5), 146.58 (C-7), 140.77 (C-9), 140.13 (C-10), 134.83 (C-6'), 127.03 (C-1'), 125.25 (C-7'), 123.72 (C-6), 123.12 (C-8'), 122.07 (C-10'),

119.39 (C-9'), 111.42 (C-5') ppm; m. p. 347.1-347.4°C. $C_{16}H_{10}N_4O_2$ (290.28): calcd. C 66.20, H 3.47, N 19.30, found C 66.10, H 3.26, N 19.29.

5.3.3 *Synthesis of compounds 5 and 6*

To a solution of anthranilamide (1.0 mmol; 1.0 equiv.) and *p*-TsOH (0.05 mmol) in THF (10 mL) was added the appropriate aldehyde (1.2 mmol; 1.2 equiv.). The mixture was stirred at room temperature for 2 hours, and then I_2 (1.5 mmol) was added. After stirring at rt for 3 hours, the excessive iodine was removed by adding $Na_2S_2O_3$ aqueous solution, and the product was extracted with CH_2Cl_2. The combined organic layer was washed with brine, dried over Na_2SO_4 and the solvent was evaporated under reduced pressure. The crude residue was purified by recrystallization from CH_3OH.

5.3.3.1. *2-(Pyridin-2-yl)quinazolin-4(3H)-one (5)*

Following general procedure compound **5** was obtained as a white solid, yield, 72%; colourless powder; m. p. 168.1-168.4 °C (lit.[5S] 168.3–169.4 °C). The spectroscopic data were in good agreement with the literature: ^{1}H NMR: ($CDCl_3$, 600 MHz): δ 10.98 (s, 1H, NH), 8.68 (d, *J* = 4.8 Hz, 1H, H-5'), 8.62 (d, *J* = 7.9 Hz, 1H, H-2'), 8.36 (dd, *J* = 8.0, 1.0 Hz, 1H, H-5), 7.93 (dt, *J* = 7.8, 1.7 Hz, 1H, H-3'), 7.85 (d, *J* = 7.9 Hz, 1H, H-8), 7.81 (dt, *J* = 7.8, 1.5 Hz, 1H, H-7), 7.53 (dt, *J* = 7.5, 1.2 Hz, 1H, H-6), 7.50 (ddd, *J* = 7.5, 4.8, 1.1 Hz, 1H, H-4') ppm. ^{13}C NMR: ($CDCl_3$, 150.9 MHz): δ 161.33 (CO), 148.98 (C-2), 148.92 (C-1'), 148.72 (C-5'), 148.26 (C-9), 137.52 (C-3'), 134.59 (C-7), 127.94 (C-8), 127.32 (C-6), 126.75 (C-5), 126.27 (C-4'), 122.42 (C-10), 122.03 (C-2') ppm. [6S] $C_{13}H_9N_3O$ (223.23): calcd. C 69.95, H 4.06, N 18.82, found C 69.82, H 4.05, N 19.02.

5.3.3.2 *2-(Quinoline-2-yl)quinazolin-4(3H)-one (6)*

Following general procedure compound **6** was obtained as a white solid, yield, 61%. The spectroscopic data were in good agreement with the literature.[7S] ^{1}H NMR: ($CDCl_3$, 600 MHz): δ 11.23 (s, 1H, NH), 8.67 (d, *J* = 8.5 Hz, 1H, H-2'), 8.39 (dd, *J* = 7.9, 1.7 Hz, 1H, H-5), 8.37 (d, *J* = 8.5 Hz, 1H, H-3'), 8.17 (d, *J* = 8.5 Hz, 1H, H-7'), 7.92-7.89 (m, 2H, H-8; H-4'), 7.84-7.80 (m, 2H, H-7; H-6'), 7.66 (dt, *J* = 7.5, 0.9 Hz, 1H, H-5'), 7.55 (dt, *J* = 7.5, 0.9 Hz, 1H, H-6) ppm. ^{13}C NMR: ($CDCl_3$, 150.9 MHz): δ 161.40 (CO), 149.05 (C-2), 148.95 (C-1'), 147.99 (C-9), 146.74 (C-8'), 137.62 (C-3'), 134.60 (C-7), 130.49 (C-6'), 129.65 (C-7'), 129.27 (C-9'), 128.27 (C-5'), 128.19 (C-8), 127.74 (C-4'), 127.56 (C-6), 126.77 (C-5'), 122.62 (C-10), 118.43(C-2') ppm; m. p. 227.7-227.9 °C (lit.[7S] 267-268 °C). Melting temperatures are significantly divergent with literature values, possibly due to polymorphism. $C_{17}H_{11}N_3O$ (273.29): calcd. C 74.71, H 4.06, N 15.38, found C 74.91, H 4.26, N 15.10.

5.4. Computational methods

For computational design purposes, we use several procedures, ranging from molecular graphics, [39] to all-electron wave function theory, WFT, using default structure optimization procedures in the Gaussian 09 program system.[48] SCS-MP2 structure optimization procedures and single point RIMP2 calculations are carried out using default convergence criteria in GAMESS-US.[49] Computations at the 6-31G(d,p) basis set level are used throughout, unless stated otherwise, along with the SVP auxiliary basis set for RIMP2. [49, 57] Density functional theory, DFT, [50] calculations are carried out with Gaussian 09 default unconstrained energy minimization procedures and convergence criteria as well. Molecular dynamics simulations are done with the software package GROMACS 2018.6[51] with the CHARMM27[52] force field.

5.5. Cells and cell culture

MDA-MB-231 (ECACC catalogue no. 92020424) epithelial, human breast cancer cell line has been used in all experiments for establishing the biological activity of phthalimido-substituted quinazolinone and its aza-analogue (compounds 1 and 2); schizocommunin (compound 3), its aza-schizocommunin analogue (compound 4) and compounds 5 and 6, quinazolin-4-ones substituted directly with a heterocyclic fragment. The cells have been maintained in DMEM medium supplemented with 10% foetal calf serum and 100 U ml^{-1} penicillin and 100 µg ml^{-1} streptomycin solution at 37°C in a fully humidified atmosphere at 5% CO_2. Cells were incubated with the tested compounds at concentration of 30, 75 and 150 µg/ml (f.c.) for 4 hours at optimal conditions and have thereafter been subjected to analyses for their potential biological activities. For all biological analyses the adherent cells were detached using a mixture of 0.05% trypsin and 0.02% EDTA.

5.6. Single-cell gel electrophoresis (SCGE)

Briefly, $1x10^3$ cells were mixed with 0.7% (f.c.) of low-gelling agarose and were layered as microgels on microscopic slides. Slides were then lysed in 146 mM NaCl, 30 mM EDTA, pH7, 10 mM Tris-HCl, pH7 and 0.1% N-lauroylsarcosine at 10°C for 20 min and were electrophoresed for 20 min at 0.46 V/cm (Molecular probes). Results were visualized under a fluorescent microscope after staining of gels with SYBR green. Results were quantified by Comet Assay specialized software CometScore. Comet images have been taken

with Olympus 8μ camera. Images have been processed on Photoshop CC 2018. Three repetitions of the experiment have been done and results are processed on Excel 2016.

5.7. FACS analysis

FACS was performed on MDA cells fixed with 76% of cold ethanol immediately after incubation with the tested compounds and left at -20°C for 24 hours in order the cells to be fixed. After fixation cells were pelleted by centrifugation, washed in PBS buffer and treated with 100 μg/ml RNAse A for 30 min at 37°C followed by staining with 50 μg/ml of propidium iodide for 30 min in the dark. 100 000 cells were counted through flow cytometry, detecting red fluorescence at excitation wavelength of 488 nm. Light scattering was detected as well. The results were quantified by FlowJo V10 and graphically presented via means of Excel 2016. Three repetitions of the experiment have been done and results are statistically analysed.

Acknowledgements: This work has been supported by the Bulgarian Science Fund, via Grant Number DN 19/11 of Dec. 10, 2017. The funding organization, www.fni.bg, has not been otherwise involved in the study design, data collection and report writing. Most reported computations have been carried out on the AVITOHOL HPC cluster facility, https://www.top500.org/system/178609, last accessed Sep. 01, 2020.

Authors' conflict of interest: None declared.

Roles of All Authors

Jose Kaneti: Computational modeling; Writing and editing of the computational part.

Milena Georgieva: Conceptualization, Methodology and Data analysis and Curation for genotoxicity results of the studied materials, Writing and Editing of the biological part.

Miroslav Rangelov: MD simulations.

Irena Philipova : Synthesis and characterization of the studied compounds.

Ivan Angelov: Fluorescence experiments.

Bela Vasileva: Methodology and Experimental design of genotoxicity testing.

Dessislava Staneva: FACS data curation.

George Miloshev: Supervision, Writing and Reviewing of the biological part.

Snezhana Bakalova: Computational modeling; Writing, Reviewing and Editing

of the manuscript.

References

1. He, L.; Li, H.; Chen. J.; Wu, X.-F. Recent Advances in 4(3H)-Quinazolinone Syntheses, *RSC Advances* **2014**, *4*, 12065-12077.
2. Tiwary, B. K.; Pradhan, K.; Nanda, A. K.; Chakraborty, R. Implication of Quinazoline-4(3H)-ones in Medicinal Chemistry: A Brief Review**.** *J. Chem. Biol. Ther.* **2015**, *1*: 104.
3. Hameed, A.; Al-Rashida, M.; Uroos, M.; Syed, A. A.; Ishtiaq, M.; Khan, K. M. Quinazoline and quinazolinone as important medicinal scaffolds: a comparative patent review (2011–2016), *Expert Opinion on Therapeutic Patents*, **2018**, *28*, 281-297.
4. von Niementowski, S. Synthesen von Chinazolinverbindungen. *J. Prakt. Chem*. **1895**, *51*, 564-572.
5. Lee, E. S. ; Son, J. K.; Na, Y. H.; Jahng, Y. Synthesis and Biological Properties of Selected 2-aryl-4(3H)-quinazolinones. *Heterocycl. Comm.* **2004**, *10*, 325-330.
6. Philipova, I.; Dobrikov, G.; Kurtova, K.; Kaneti, J. Convenient synthesis of some 2-substituted 4(3H)-quinazolinone derivatives. *J. Heterocyclic Chem.* **2006**, *43*, 1057-1063.
7. Uehata, K.; Kimura, N.; Hasegawa, K.; Shigeru, A.; Nishida, M.; Hosoe, T.; Hawai, K.; Nishida, A. Total Synthesis of Schizocommunin and Revision of Its Structure. *J. Nat. Prod.* **2013**, *76*, 2034-2039.
8. Che, T.; Chen, S. B.; Tu, J. L.; Wang, B.; Zhang, Y.; Wang, J.; Wang, Z. Q.; Zhang, Z. P.; Ou, T. M.; Zhao, Y.; Tan, J. H.; Huang, Z. S. Discovery of Novel Schizocommunin Derivatives as Telomeric G-Quadruplex Ligands That Trigger Telomere Dysfunction and the Deoxyribonucleic Acid (DNA) Damage Response. *J. Med. Chem.* **2018**, *61*, 3436-3453.
9. Dempsey, R. O.; Skibo, E. B. Rational design of quinazoline-based reversible inhibitors of human erythrocyte purine nucleoside phosphorylase, Biochemistry **1991**, 30, 8480-8487.
10. Davoll, J.; Johnson, A. M. Quinazoline analogues of folic acid. *J. Chem. Soc. C*, **1970**, *8*, 997-1002.
11. Scanlon, K. J.; Moroson, B. A.; Bertino, J. R.; Hynes, J. B. Quinazoline Analogues of Folic Acid as Inhibitors of Thymidylate Synthetase from Bacterial and Mammalian Sources. *Mol. Pharmacol.* **1979**, *16*, 261-269.
12. Che, T.; Wang, Y.-Q.; Huang, Z.-L.; Tan, J. H.; Huang, Z.-S.; Chen, S.-B. Natural Alcaloids and Heterocycles as G-Quadruplex Ligands and Potential Anticancer Agents. *Molecules* **2018**, 23, 493.
13. Bajpayee, M.; Kumar, A.; Dhawan, A. The comet assay: assessment of in vitro and in vivo DNA damage. *Methods in molecular biology*, **2013**, *1044*, 325-345.
14. Collins, A. R. The comet assay: a heavenly method! *Mutagenesis*, **2015**, *30*(1), 1-4.

15. Georgieva, M.; Zagorchev, P.; Miloshev G. Random, double- and single-strand DNA breaks can be differentiated in the method of Comet assay by the shape of the comet image. *Electrophoresis* **2015**, *36*(20), 2553-2560.
16. Fairbairn, D.W.; Olive, P. L.; O'Neill, K. L. The comet assay: a comprehensive review. *Mutation research* **1995**, *339*(1), 37-59.
17. Hartmann, A.; Agurell, E.; Beevers, C.; Brendler-Schwaab, S.; Burlinson, B.; Clay, P.; Collins, A.; Smith, A.; Speit, G.; Thybaud, V. Recommendations for conducting the in vivo alkaline Comet assay, 4th International Comet Assay Workshop. *Mutagenesis* **2003**, *18*(1), 45-51.
18. Tice, R. R.; Agurell, E.; Anderson, D.; Burlinson, B.; Hartmann, A.; Kobayashi. H.; Miyamae, Y.; Rojas, E.; Ryu, J. C.; Sasaki, Y. F. Single cell gel/comet assay: guidelines for in vitro and in vivo genetic toxicology testing. *Environmental and molecular mutagenesis* **2000**, *35*(3), 206-221.
19. Peycheva, E.; Georgieva, M.; Miloshev, G. Comparison Between Alkaline and Neutral Variants of Yeast Comet Assay. *Biotechnology & Biotechnological Equipment* **2009**, *23*(1), 1090-1092.
20. Olive, P. L.; Banáth, J. P. The comet assay: a method to measure DNA damage in individual cells. *Nature protocols* **2006**, *1*, 23-29.
21. Georgieva, M.; Staneva, D.; Uzunova, K.; Efremov, T.; Balashev, K.; Harata, M.; Miloshev, G. The linker histone in Saccharomyces cerevisiae interacts with actin-related protein 4 and both regulate chromatin structure and cellular morphology. *Int. J. Biochem. Cell Biol.* **2015**, *59*, 182-192.
22. Alvarez, D. F.; Helm, K.; Degregori, J.; Koederer, M.; Majka, S. Publishing flow cytometry data. *American journal of physiology Lung cellular and molecular physiology*, **2010**, *298*(2), L127-L130.
23. Gay, L.; Baker, A.-M.; Graham, T. A. Tumour Cell Heterogeneity. **2016**, *F1000Research. 5:F1000 Faculty Rev-*1238; doi: 10.12688/f1000research.7210.1
24. Mhaske, S. B.; Argade, N. P. Regioselective Quinazolinone-Directed Ortho Lithiation of Quinazolinoylquinoline: Practical Synthesis of Naturally Occurring Human DNA Topoisomerase I Poison Luotonin A and Luotonins B and E. *J. Org. Chem.* **2004**, *69*, 4563-4566.
25. Wang, K.-B.; Elsayed, M.; Wu, G.; Deng, N.; Cushman, M.; Yang, D. Indenoisoquinoline Topoisomerase Inhibitors Strongly Bind and Stabilize the MYC Promoter G-Quadruplex and Downregulate MYC. *J. Am. Chem. Soc.* **2019**, *141 (28)*, 11059-11070.
26. Xie, Y.; Tam, Y. K.; Tor, Y. The interactions of Small Molecules with DNA and RNA, in *The Chemical Biology of Nucleic Acids*, Ed. by Mayer, G. **2010**, 115-140.
27. Gago, F. Stacking Interactions and Intercalative DNA Binding. *METHODS: A companion to Methods in Enzymology* **1998**, 14, 277-292.
28. Yu, H.-Q.; Miyoshi, M.; Sugimoto, N. Characterization of Structure and Stability of Long Telomeric DNA G-Quadruplexes, *J. Am. Chem. Soc.* **2006**, *128*, 15461-15468.
29. Rhodes, D.; Lipps, H. J. G-quadruplexes and their regulatory roles in biology. *Nucl. Acid Res.* **2015**, 43, 8627-8637. doi: 10.1093/ nar/gkv862
30. Clark, G. R.; Pytel, P. D.; Squire, C. J.; Neidle, S. Structure of the First Parallel DNA Quadruplex-Drug Complex, *J. Am. Chem. Soc.* **2003**, *125*, 4066-4067.
31. Li, Z.; Tan, J.-H.; He, J.-H.; Long, Y.; Ou, T.-M.; Li, D.; Gu L.-Q.; Huang, Z.-S. Disubstituted Quinazoline Derivatives as a New Type of Highly Selective Ligands for Telomeric G-Quadruplex DNA, *Eur. J. Med. Chem.* **2012**, *47*, 299-311.
32. Di Fonzo, S.; Amato, J.; D'Aria, F.; Caterino, M.; D'Amico, F.; Gessini, A.; Brady, J. W.; Cesaro, A.; Pagano, B.; Giancola, C. Ligand binding to G-quadruplex DNA: new insights

from ultraviolet resonance Raman spectroscopy, *Physical Chemistry Chemical Physics* **2020**, *22*, 8128-8140; https://doi.org/10.1039/D0CP01022G .
33. Mazzini, S.; Gargallo, R.; Musso, L.; De Santis, F.; Aviño, A.; Scaglioni, L.; Eritja, R.; Di Nicola, M.; Zunino, F.; Amatulli, A.; Dallavalle, S. Stabiization of c-KIT G-Quadruplex DNA Structures by the RNA Polymerase I Inhibitors BMH-21 and BA-41, *Int. J. Mol. Sci.* **2019**, *20*, 4927-4944.
34. Clay, E. H.; Gould, I. R. A Combined QM and MM Investigation into Guanine Quadruplexes, *J. Mol. Graphics and Modelling*, **2005**, *24*, 138-146.
35. Yurenko, Y. P.; Novotny, J.; Sklenar, V.; Marek, R. Exploring non-covalent interactions in guanine and xanthine-based model DNA quadruplex structures: a comprehensive quantum chemical approach, *Phys. Chem. Chem. Phys.* **2014**, *16*, 2072-2084.
36. Poudel, L.; Steinmetz, N. F.; French, R. H.; Parsegian, V. A.; Podgornik, R.; Ching, W.-Y. Implications of the Solvent Effect, Metal Ions and Topology in the Electronic Structure and Hydrogen Bonding of Human Telomeric G-quadruplex DNA. *Phys. Chem. Chem. Phys.* **2016**, *18*, 21573-21585.
37. Machireddy, B.; Sullivan, H.-J.; Wu, C. Binding of BRACO19 to a Telomeric G-Quadruplex DNA Probed by All-Atom Molecular Dynamics Simulations with Explicit Solvent. *Molecules* **2019**, *24*, 1010, https://doi.org/10.3390/molecules24061010.
38. Neidle, S. Quadruplex Nucleic Acids as Novel Therapeutic Targets. *J. Med. Chem.* **2016**, *59*, 5987−6011.
39. MOLDEN: Schaftenaar, G. http://cheminf.cmbi.ru.nl/molden/; VMD: https://www.ks.uiuc.edu/ Research/vmd/
40. Stewart J. J. P., MOPAC2016, Stewart Computational Chemistry, Colorado Springs, CO, USA, HTTP://OpenMOPAC.net, **2016**. Last accessed: Sep. **2019**.
41. Pople, J. A.; Raghavachari, K.; Schlegel, H. B.; Binkley, J. S. *Int. J. Quantum Chem., Quant. Chem. Symp.*, **1979**, *S13*, 225-41; Grimme, S. Improved second-order Møller–Plesset perturbation theory by separate scaling of parallel- and antiparallel-spin pair correlation energies. *J. Chem. Phys.* **2003**, *118*, 9095-9102.
42. Chai, J.-D.; Head-Gordon, M. Long-range corrected hybrid density functionals with damped atom–atom dispersion corrections. *Phys. Chem. Chem. Phys.* **2008**, *10*, 6615-6620.
43. Hobza, P. and Šponer, J. Toward True DNA Base-Stacking Energies: MP2, CCSD(T) and Complete Basis Set Calculations, *J. Am. Chem. Soc.* **2002**, *124*, 11802-11808.
44. Kruse, H.; Banaš, P.; and Šponer, J. Investigations of Stacked DNA Base Steps: Highly Accurate Stacking Interaction Energies, Energy Decomposition, and Many-Body Stacking Effects, *J. Chem. Theor. Comput.* **2019**, *15*, *1*, 95-115.
45. Mo, Y. Probing the nature of hydrogen bonds in DNA base pairs, *J. Mol. Model.* **2006**, *12*, 665-672.
46. Malgowska, M.; Czajczinska, K.; Gudanis, D.; Tvorak, A. and Gdaniec, Z. Overview of the RNA G-Quadruplex Structures, *Acta Biochim. Polon*. **2016**, *63*, 609-621.
47. Kogut, M.; Kleist, C.; Czub, J. Molecular dynamics simulations reveal the balance of forces governing the formation of a guanine tetrad - a common structural unit of G-quadruplex DNA, *Nucl. Acid Res.* **2016**, *44*, 3020-3030.
48. GAUSSIAN 09, v. D.01; Frisch, M. J.; Trucks, G. W.; Schlegel, H. B.; Scuseria, G. E.; Robb, M. A.; Cheeseman, J. R.; Scalmani, G.; Barone, V.; Mennucci, B.; Petersson, G. A.; Nakatsuji, H.; Caricato, M.; Li, X.; Hratchian, H. P.; Izmaylov, A. F.; Bloino, J.; Zheng, G.; Sonnenberg, J. L.; Hada, M.; Ehara, M.; Toyota, K.; Fukuda, R.; Hasegawa, J.; Ishida, M.; Nakajima, T.; Honda, Y.; Kitao, O.; Nakai, H.; Vreven, T.; Montgomery, Jr., J. A.; Peralta, J. E.; Ogliaro, F.; Bearpark, M.; Heyd, J. J.; Brothers, E.; Kudin, K. N.; Staroverov, V. N.; Keith, T.; Kobayashi, R.; Normand, J.; Raghavachari, K.; Rendell, A.; Burant, J. C.; Iyengar, S. S.; Tomasi, J.; Cossi, M.; Rega, N.; Millam, J. M.; Klene, M.; Knox, J. E.; Cross,

J. B.; Bakken, V.; Adamo, C.; Jaramillo, J.; Gomperts, R.; Stratmann, R. E.; Yazyev, O.; Austin, A. J.; Cammi, R.; Pomelli, C.; Ochterski, J. W.; Martin, R. L.; Morokuma, K.; Zakrzewski, V. G.; Voth, G. A.; Salvador, P.; Dannenberg, J. J.; Dapprich, S.; Daniels, A. D.; Farkas, O.; Foresman, J. B.; Ortiz, J. V.; Cioslowski, J.; Fox, D. J. Gaussian, Inc., Wallingford, CT, **2013**.

49. GAMESS-US: Schmidt, M.W.; Baldridge, K.K.; Boatz, J.A.; Elbert, S.T.; Gordon, M.S.; Jensen, J.H.; Koseki, S.; Matsunaga, N.; Nguyen, K.A.; Su, S.J.; Windus, T.L.; Dupuis, M.; Montgomery J.A. *J. Comput. Chem.* **1993**, *14*, 1347-1363. Last accessed: Dec. 06, **2019**.

50. Koch, W.; Holthausen, M. C. A Chemist's Guide to Density Functional Theory. Second Edition, Wiley-VCH Verlag GmbH, **2001**.

51. GROMACS 2018.6 with the NA force field from MacKerell Jr, A. D.; Banavali, N.; Foloppe, N. Development and current status of the CHARMM force field for nucleic acids. *Biopolymers*, **2001**, *56(4)*, 257-265.

52. MacKerell, A. D. Jr.; Banavali, N.; Foloppe N. Development and current status of the CHARMM force field for nucleic acids, *Biopolymers*. **2001**, *56:4*, 257–265.

53. Caprio, V.; Guyen, B.; Opoku-Boahen, Y.; Mann, J.; Gowan, S.M.; Kelland, L.M.; Read, M.A.; Neidle, S. A novel inhibitor of human telomerase derived from 10H-indolo[3,2-b]quinoline. *Bioorg. Med. Chem. Lett.* **2000**, *10*, 2063–2066.

54. Perry, P. J.; Gowan, S. M.; Read, M. A.; Kelland, L. R.; Neidle, S. Design, Synthesis and Evaluation of Human Telomerase Inhibitors Based Upon a Tetracyclic Structural Motif, *Anti-Cancer Drug Design* **1999**, *14*, 373-382.

55. Neidle, S. Quadruplex Nucleic Acids as Novel Therapeutic Targets, *J. Med. Chem.* **2016**, 59, 5987-6011.

56. Feyereisen, M.; Fitzgerald, G.; Komornicki, A. Use of approximate integrals in ab initio theory. An application in MP2 energy calculations: *Chem. Phys. Lett.* **1993**, *208* (5-6), 359-363.

57. Chen, S.B.; Tan, J.H.; Ou, T.M.; Huang, S.L.; An, L.K.; Luo, H.B.; Li, D.; Gu, L.Q.; Huang, Z.S. Pharmacophore-based discovery of triaryl-substituted imidazole as new telomeric G-quadruplex ligand. *Bioorg. Med. Chem. Lett.* **2011**, *21*, 1004–1009.

58. Vy Thi Le, T.; Han, S. H.; Chae, J.; Park, H.-J. G-Quadruplex Binding Ligands: from Naturally Occurring to Rationally Designed Molecules, *Curr. Pharm. Design* **2012**, *18*, 1948-1972.

59. Haider, J. Computational methods to study G-quadruplex – ligand complexes, *J. Indian Inst. Sci.* **2018**, *98:3*, 325-339.

60. N. Panera, A. Tozzi, A. Alizi, The G-quadruplex/helicase world as potential antiviral approach against COVID 19, DOI: 10.21203/rs.3.rs-21609/v1.

Highligths

- 2-vinyl-quinazolin-4-ones (V2Qs) are moderate MDA breast cancer cell suppressors
- Probable mechanism of V2Qs' action is stacking to telomeric G-quadruplexes
- Computed DFT and RI-MP2 stacking energies reproduce observed trends in genotoxicity
- Heterocycle-quadruplex stabilization energy may be used for prediction of activity